Influence of Solar Activity Cycles on Earth's Climate

Task 3 – Data Interpretation
Task 4 – Quantification of global climate modulations

WP301 – Data Interpretation Earth Surface
WP302 – Data Interpretation Troposphere
WP401 – Quantification Earth Surface
WP402 – Quantification Troposphere

N. Marsh, H. Svensmark, F. Christiansen, and T. Bondo
Danish National Space Center

June 23, 2006

Contents

INTRODUCTION....3

SOLAR MODULATED FORCING PARAMETERS....5

INTERNAL MODES OF VARIABILITY....8

ANALYSIS METHOD....10

TROPOSPHERIC RESPONSE....12

- TEMPERATURE....12
- SOLAR MAX/MIN....18
- VERTICAL CIRCULATION....25
- LOW CLOUDS....27
- OZONE....31
- AEROSOLS....33

SURFACE RESPONSE....35

- VEGETATION....35
- SNOW....37
- SEA ICE....39
- PRECIPITATION....41
- SURFACE PRESSURE....42
- SURFACE TEMPERATURE....44

SUMMARY....48

REFERENCES....50

Introduction

The goal of this Task is to describe the response of global climate to solar modulated forcing parameters. This report is a review of the work performed during Task 3 and Task 4 at DNSC, where we have integrated the work packages WP301, WP302, WP401 and WP402 that specifically focus on the response in the Troposphere and at Earth's Surface. The ISAC team requested in September 2005 that Task 3 (Data interpretation) be combined with Task4 (Quantification of global climate modulations). This was due to the fact that the activities under Task 3, which included a) the conversion of satellite instrument observations into geophysical observations, b) validation of satellite data with in-situ data, and c) the identification and analysis of discrepancies, had largely been carried out by the Data providers themselves. The ISAC team are very much "end users" of this data and it was felt that the time could be spent more profitably in analyzing the data within the context of solar variability.

The atmospheric response to solar variability will be characterised at various time-scales by comparing solar modulated forcing parameters with the climate parameters identified in Task 2 (see WP202 and WP203). By identifying the nature of the climate response both temporally and spatially, it will be possible to place constraints on potential physical mechanisms that may link changes in Earth's climate to solar variability. The correlation statistic and multiple-regression analysis are the key tools used in this project, together with estimates of significance taking account of any serial autocorrelations that may be present. In the following review only the key results from the correlation analysis will be presented; interpretation in the context of the relevant mechanisms will be described in Task 5.

It was previously noted that there is little difference in the phase between the various solar modulated forcing parameters over a solar cycle (WP103). As a result, it will be difficult to determine the solar modulated process responsible for any significant response found in the climate data at time scales where the effects of the solar cycle dominate. In an attempt to account for this, the effects of the solar cycle were removed from the data using two techniques; 1) via multiple-regression where the solar cycle is represented by the sunspot number and, 2) by selecting narrow periods around solar max and solar min where the effects of the solar cycle are almost stationary. This allowed for a comparison of fluctuations in the data at higher frequencies than the solar cycle. A cursory glance at the solar modulated forcing parameters in Figure 1 indicates that the amplitude of fluctuations around the solar cycle are much larger under solar maximum than solar minimum conditions. These fluctuations, which are generally independent for each forcing parameter, e.g., forbush decreases, ground level events, solar flares etc., provide a possible means to distinguish between the different processes. However, the solar processes are highly variable at time-scales of hours to days. This makes the task of identifying a solar signal in the climate data more involved since, at these timescales, fluctuations in local weather phenomena and internal climate variations are often large and can mask the solar effect being explored. This is likely to have a strong impact on the data analysis. So there is a trade-off between the need to resolve short term fluctuations, possibly driven by solar variability, above the internal noise of the climate system. The data used in the following analysis is therefore limited to monthly averages,

which reduces the climatic noise, but also allows for an analysis of high frequency fluctuations around the solar cycle.

Another important consideration is the effect of internal climate variability at decadal time scales and the impact from volcanoes. Since these processes can have a strong impact on many climate parameters in the troposphere and at the surface, they could mask, or artificially enhance, a possible solar cycle signal with an average length around 11 years. To reduce this problem, temporal indices describing the variability from El Nino Southern Oscillation (ENSO), North Atlantic Oscillation (NAO) and Volcanic Stratospheric Aerosol have also been included in the multiple regression analysis. It is entirely possible that these internal climate modes are themselves modulated by solar variability, and this is determined before performing the multiple-regression.

The report is structured as follows. Initially the five solar modulated forcing parameters and three internal modes of climate variability are briefly presented. Then follows a short description of the common methods used throughout the analysis. The detailed review of the analysis itself is divided into two sections one describing tropospheric parameters (including temperature, vertical winds, low clouds, aerosols, and ozone) and one describing surface parameters (including vegetation, snow, precipitation, and surface pressure). Finally the major findings are summarised for use in the remaining ISAC Tasks.

Solar Modulated Forcing Parameters

In the first two Tasks (WP101, WP102, WP201, WP202) the ISAC team identified five external forcing parameters that are modulated by solar variability and have the potential to influence Earth's lower atmosphere below 50km. Below a brief definition is provided of the parameters that have been identified: Total Solar Irradiance (TSI), the Ultra-Violet (UV) component of solar radiation, Galactic Cosmic Rays (GCR), the direct input from the Solar Wind (SW), and the total Hemispheric Power Input (HPI) reflecting properties of precipitating particles within the magnetosphere. The five parameters are plotted in Figure 1.

Total Solar Irradiance (TSI) in Figure 1a describes the integrated radiant energy arriving from the sun at the top of Earth's atmosphere. Direct observations of TSI have been obtained from six consecutive Earth orbiting satellite's that have been inter-calibrated to provide a continuous time series from 1978 – 2005 (Frohlich and Lean, 2002). A number of reconstructions of TSI before 1978 are also available based on a range of solar proxies. While these reconstructions generally agree that solar radiative output has increased by ~1.7 Wm^{-2} over the past century (see section 3.0 WP 103 or Lockwood (2002)), there are large uncertainties at time scales of months to years which describe the amplitude and short term fluctuations over a solar cycle. Thus where TSI is involved, the analysis has been limited to the period 1978-2005 when satellite observations were available.

The Ultra-Violet (UV) component of solar radiation in Figure 1b is obtained from the MgII absorption line, which describes the properties of the UV radiation at wavelengths around 280nm (Deland and Cebula, 1993;Viereck and Puga, 1999). These wavelengths penetrate deep into the middle stratosphere below 50km altitude (see section 3.0 WP 103). The UV observations are obtained from the same satellites as TSI and so are also available over the period 1978-2005. Prior to 1978, it is possible to use the 10.7 cm radio flux, obtained from ground stations, to produce an index for the Extreme Ultra-Violet (EUV – wavelengths ~20-30nm) component of solar radiation (see WP201 and Tobiska (2001)). Although used as a proxy, the 10.7cm flux is governed by processes on the sun that are similar to those generating EUV. At timescales of months to years EUV is in very close agreement with UV where the two sets of observations overlap, see Figure 1b. This provides confidence when using EUV to extend estimates of UV variations back until 1947.

The direct input from the Solar Wind (SW), Figure 1c, is represented by the product between the solar wind speed, v_{sw}, and the southward component of the Interplanetary Magnetic Field (IMF), B_z. Only the southern polarity is included since this is the most efficient configuration for transferring energy directly from the solar wind to the Earth's magnetosphere. Solar wind properties, including v_{sw} and B_z, have been observed in-situ from 1963 until present by various satellite missions including: IMP, WIND, ISEE, ACE, and CELIAS/MTOF (see WP201 for details). Through its coupling with the magnetosphere the solar wind drives ionospheric currents at high latitudes depositing Joule heating in the upper atmosphere (above 100km) which may have the potential to accelerate the denser atmosphere below.

The total Hemispheric Power Input (HPI), Figure 1d, indicates the amount of energy deposited over an entire hemisphere in the upper atmosphere by precipitating particles

measured inside the magnetosphere. The precipitating particles have various sources, foremost directly from the solar wind and from the tail of the Earth's magnetosphere during magnetic (sub-)storms. The particles mainly dump their energy at high latitudes at ionospheric heights. The HPI parameter is given as total energy deposited during a satellite pass and is derived from the high latitude precipitating flux that has been continuously monitored by the NOAA/TIROS and DMSP satellites over the period 1978-2003 (Foster et al., 1986;Fullerrowell and Evans, 1987). This is the most speculative of the solar modulated forcing parameters as the energies involved are extremely small, and currently no amplification mechanism exists that could explain a significant link with the denser atmosphere below.

Galactic Cosmic Rays (GCR), Figure 1e, are represented by the monthly averaged hourly neutron counts from the ground station at Climax (39N, 106W, 3400m, Geomagnetic vertical cut-off = 3.03 GeV) (University of New Hampshire, "National Science Foundation Grant ATM-0339527"). Neutron monitors are sensitive to the number of secondaries generated when high energy cosmic rays (protons and alpha particles) collide with atmospheric nuclei and create a cascade of charged particles that are the main source of ionization in the lower part of the atmosphere below 35 km. The number of cosmic rays entering the Earth's atmosphere is modulated by both the solar wind and the Earth's magnetic field. Ionization from GCR possibly influences the atmospheric aerosol distribution on which clouds form, and/or affects the global atmospheric electric circuit with the potential to enhance collision efficiencies at cloud boundaries (see section 3.3, WP 103). The station at Climax has monitored GCR continuously from 1953 to present (University of New Hampshire, "National Science Foundation Grant ATM-0339527").

The effect of the solar cycle on these five parameters is clearly visible from the correlation coefficients, (Table 1), with sunspot number (SSN). Also indicated are the correlation coefficients between the five solar modulated parameters before removal of the solar cycle (above the diagonal, bold face), after removal of the solar cycle (below the diagonal, normal type), and between each solar modulated parameter before and after removal of the solar cycle (diagonal, italics).
Note that SW and in particular HPI, display the weakest correlation with both SSN and the other parameters. This feature will be useful in the following analysis when distinguishing between different solar modulation effects.

	TSI	UV	EUV	SW	HPI	GCR	SSN
TSI	*0.70*	**0.80**	**0.79**	**0.31**	**0.09**	**-0.63**	**0.72**
UV	0.59	*0.30*	**0.98**	**0.48**	**0.17**	**-0.79**	**0.77**
EUV	0.50	0.77	*0.27*	**0.50**	**0.19**	**-0.85**	**0.96**
SW	-0.02	-0.06	0.07	*0.87*	**0.59**	**-0.54**	**0.46**
HPI	-0.03	0.04	0.14	0.60	*0.99*	**-0.44**	**0.15**
GCR	-0.21	-0.44	-0.42	-0.29	-0.53	*0.61*	**-0.79**

Table 1: Correlation coefficients between the solar modulated forcing parameters. Above the diagonal (bold face) is given the correlations for the observed parameters. Below the diagonal (normal type) the same coefficients after removal of linear trend and the solar cycle from the parameters are shown. The diagonal shows the correlations for each parameter before and after removal of the solar cycle and linear trend.

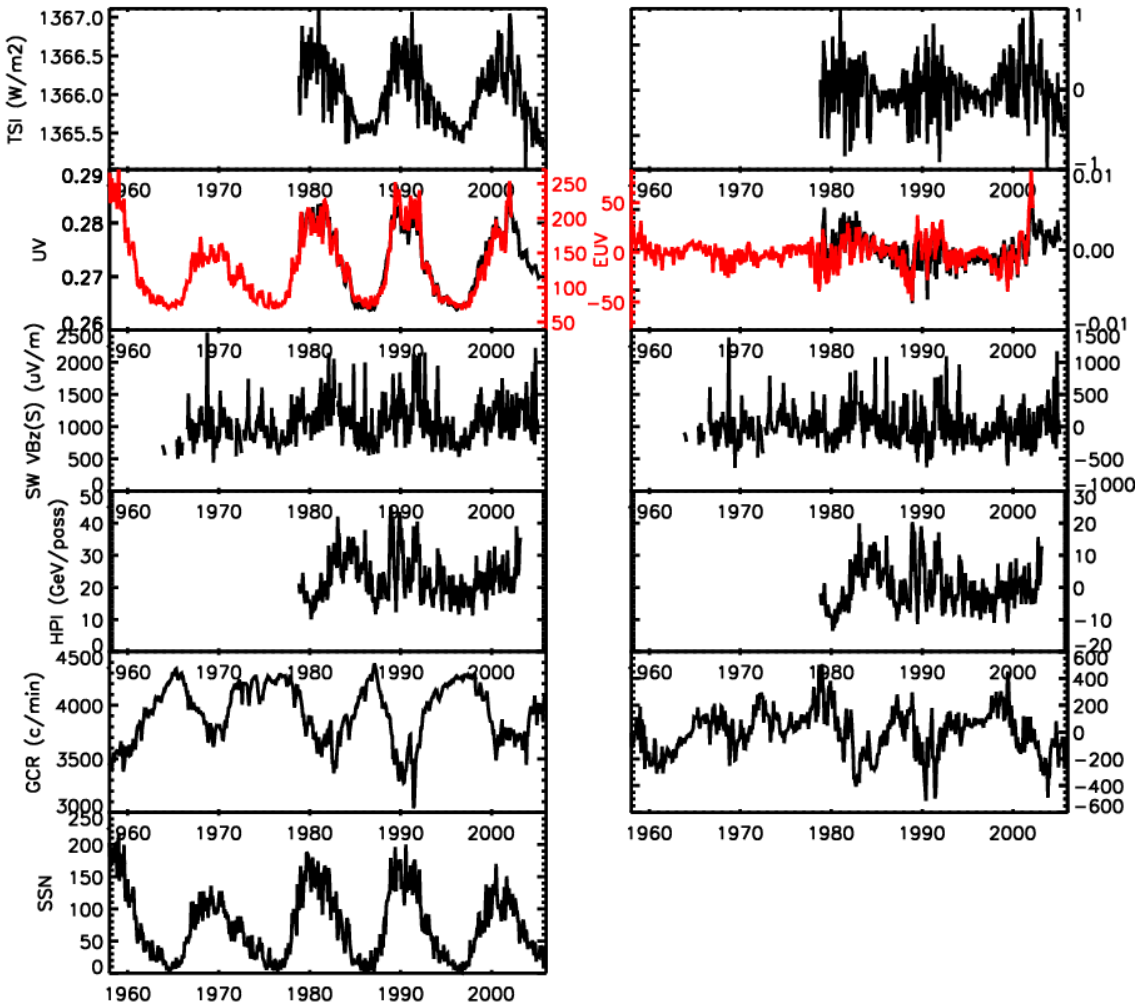

Figure 1: The five Solar Modulated Forcing Parameters over the periods where data is available. From the top a) total solar irradiance (TSI), b) solar ultraviolet radiation (UV) and the 10.7 cm proxy for extreme ultraviolet proxy (EUV - red), c) the solar wind (SW) v_swBz component for southward IMF, d), the total hemispheric power input from precipitating particles (HPI) and e) Galactic cosmic rays from the Climax station (GCR). The lowest panel (f) shows the solar activity cycle as represented by the sunspot number (SSN). To the right is shown the same parameters after removal of mean, linear trend and the solar cycle.

Internal Modes of Variability

There are a number of recurring internal modes of variability that are integral to the evolution of Earth's climate. Since a large fraction of global climate variability can be attributed to these modes, they need to be accounted for when looking for a signal of Solar modulated external forcing. Here 3 internal climate modes are considered as making a major contribution to the variability in the various climate parameters considered.

- The El Niño-Southern Oscillation (ENSO)
- The North Atlantic Oscillation (NAO)
- Volcanic Stratospheric Aerosol

Indices describing the evolution of these three internal climate modes are plotted in Figure 2, and a brief overview of the data used for each index is presented below. Further details can be found in section 6 of WP 104:

ENSO index
The periodic warming of the ocean waters west of Ecuador and Peru (El Nino) and variations in the east-west Pacific equatorial surface pressure (Southern Oscillation) are part of the same climate phenomena that falls under the common name ENSO. In a complex coupling of oceanic and atmospheric motion the rainfall associated with the shift in Sea Surface Temperature also affects regions outside of the tropics by altering global circulating wind patterns and hence global climate. ENSO occurs with a frequency of 2-5 years. The ENSO index, plotted in Figure 2a, is given by the average Sea Surface Temperatures (SSTs) anomalies over the region 5ºN-5ºS, 150º-90ºW, known as NINO3 (Wallace et al., 1998). Situated in the eastern pacific off the coast of Peru, the regions SSTs are governed by surface wind stress influencing the inclination of the thermo-cline in combination with other meteorological forcing and the impact of ocean dynamics. As surface easterlies weaken (strengthen) with the evolution of ENSO, so the inclination of the thermo-cline falls (rises) and the SSTs in the region defined NINO3 become warmer (cooler) (Peixoto and Oort, 1984). Note NINO3 is anti-correlated with SST anomalies in the western pacific over Indonesia.

NAO index
The North Atlantic Oscillation (NAO) is a large scale mode of internally driven climate variability that has a strong impact on climate and weather during the winter months in regions around the North Atlantic(Hurrell, 1995). Over decadal time-scales variability in the coupling between atmosphere and ocean leads to a see-sawing in climate regimes across northern and southern Europe, Greenland, northern Canadian and the eastern US. Evolution of the NAO, shown in Figure 2b, is often represented by an index based on the normalized difference between sea level pressure over the subtropical Azores high and subpolar Iceland low. During periods with a strong positive pressure gradient across the North Atlantic (resulting in a positive NAO index), warm and wet winters are experienced in northern Europe, and cold dry winters over Greenland and northern Canada. With a much weaker pressure gradient (resulting in a negative NAO index), northern Europe experiences cold dry winter conditions, Greenland milder temperatures, and moist air is transported over the Mediterranean. These climate shifts, particularly over decadal time scales, will have

an impact on atmospheric parameters in the North Atlantic and need to be accounted for when investigating the connection with solar variability.

Volcanic Aerosol Index (VAI)

Although not an internal mode of variability in the strict sense that the atmospheric-ocean interactions described above are, volcanoes are considered here an internal component of the Earth system since their frequency of occurrence and strength is not thought to be driven by external forcing. Volcanoes inject a huge amount of ash and gas into the stratospheric layers of the atmosphere which can take several years to fall back to the Earth's surface. This long atmospheric residence of volcanic emissions often leads to a net cooling of global climate in the years following a major eruption. Volcanoes are general thought to impact the climate through three processes; 1) particles generated during the eruption provide surfaces for ozone destroying chemical reactions to be enhanced, the climatic effect of decreasing ozone is currently not well understood; 2) Greenhouse gases such as water vapour and CO2 directly injected into the atmosphere lead to a warming; 3) large emissions of sulphur rich gases combining with water vapour in the stratosphere can produce dense clouds of sulphur droplets which block the incoming solar radiation and lead to a cooling that is much larger than either of the other effects. With three major eruptions over the past 50 years it is necessary to account for their climate effects in the data analysis that follows. The stratospheric aerosol optical thickness at 550nm is strongly effected by the input of sulphate and ash (Sato et al., 1993) and is used here as a Volcanic Aerosol Index (VAI). The data currently available (Figure 2c) stops at the end of 1999, but in the following analysis the index has been extrapolated through to 2005 with a constant background since no major eruptions occurred over this period.

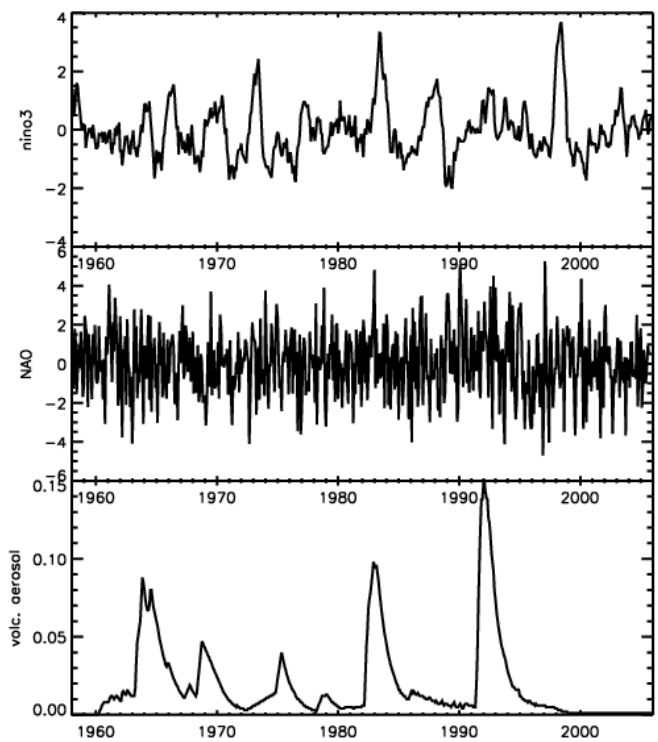

Figure 2: Internal climate modulators. From top: the nino3 index – the sea surface temperature anomaly of the tropical pacific ocean, the North Atlantic Oscillation (NOA)– the pressure difference between the Azores and Iceland, and volcanic aerosol optical thickness.

Analysis method

This section outlines the common methods used in the analysis of each of the climate parameters in the following report.

Multiple Linear Regression:

The correlation analysis is performed on the climate data and solar modulated parameters with various degrees of filtering. For each climate parameter the analysis is performed in three stages: 1) on the original observations as received from the data providers, 2) on climate observations with effects from the internal climate modes minimized, and 3) on climate and solar modulated observations with the solar cycle removed. In practice, stages 2 and 3 are performed on the residual from a multiple regression least squares fit of the data to various independent parameters. Stage 2 includes the indices describing the ENSO, NAO and Volcanoes, together with a linear trend, and is applied only to the climate data. Stage 3 additionally includes the effects of SSN which is applied to both climate data and the solar modulated parameters.

This procedure inherently assumes that the observations are linearly dependent on the 3 internal climate modes and solar modulated parameters, and that the indices themselves are independent, i.e., orthogonal. Table 2 reports the correlations between each of the indices, none of which are significantly different from the null hypothesis of no correlation, thus confirming the assumption of linear independence for monthly averages during the period 1963-2005. However, the validity of assuming a linear response is not so clear. It is well known that the nature of the climate response to El Nino was quite different during the major event of 1983 to that of 1998; this lack of stationarity needs to be borne in mind when interpreting the results. It is also possible that sensitivity to solar variability may depend on the current internal state of the climate system. A solar modulated mechanism may only be active during certain periods of the observations investigated. An attempt to address this problem is partially explored in the section comparing the solar induced response of tropospheric temperatures under solar min and solar max conditions.

	NAO	Volc.	TSI	UV	EUV	SW	HPI	GCR	SSN
Nino3	0.00	0.22	-0.05	-0.13	0.01	0.05	-0.08	-0.02	0.00
NAO		0.09	0.16	0.10	0.09	0.05	0.09	-0.05	0.09
Volc.			0.06	0.02	-0.08	0.15	0.22	-0.02	-0.09

Table 2: Correlation coefficients between solar modulated forcing parameters and the internal modes of variability.

Test of significance:
When estimating the significance of any statistical quantity, it is important to take into account any serial- (or auto-) correlations that might be present. This is especially the case when dealing with climate data where persistence is a strong feature. For example the slow evolution of a weather system over a period of days to weeks, or the waxing and waning of ocean-atmospheric coupling over a period of months to years. In the current analysis the evolution of the solar cycle is to be considered, and this possesses very strong auto-correlations effectively reducing the number of degrees of

freedom. Various techniques have been devised to account for the effective number of degrees of freedom (Angell, 1981;Ebisuzaki, 1997), in this report significance of the correlation coefficient is found by using the so called random phase test (Ebisuzaki, 1997). This requires that the probability of obtaining a correlation coefficient, r, between a specific climate parameter and solar modulated parameter by chance is found from an ensemble of Monte Carlo simulations. Each member of the ensemble consists of an artificial time series. These are generated by Fourier transforming the time series of the climate parameter in question, randomizing the phases, and then Fourier transforming back to generate a random time series which possesses the same power spectrum as the original climate parameter time series. For each random time series the correlation coefficient with the solar modulated parameters is found. This is repeated 10000 times for each ensemble, generating a probability distribution from which the significance of the original correlation coefficient can be estimated. Estimating significance by randomizing the Fourier phases in this manner is the strictest test available which accounts for any auto-correlations that are present.

Tropospheric Response

The troposphere is the inner layer of the atmosphere defined by a steady decrease of temperature with increasing altitude. Nearly all clouds and most weather phenomena felt at the surface are created in this region. In this chapter focus is placed on the following atmospheric parameters:

- Temperature
- Vertical circulation
- Low clouds.
- Ozone
- Aerosols

Temperature

Temperature is the most obvious climate parameter to focus on when considering possible climate change and also the one that has received most attention, both scientifically and in public debate. Reliable measurements of atmospheric temperatures at other levels than ground have been collected from balloon radiosonde measurements since 1958, beginning with observations from a few stations reaching thousands of stations at the present time.

The Hadley Centre of Climate Prediction and Research has compiled the radiosonde temperature measurements into a gridded data set from 1958 to present. The data are available as monthly temperature anomalies at 9 pressure levels [850, 700, 500, 300, 200, 150, 100, 50, 30hPa] on a 5-degree latitude and 10-degree longitude grid. For the analysis in this section the internal modes of variability have been subtracted from the temperature data by multi-linear-regression and the temperature data been recomputed as latitude zones containing monthly means of the anomalies

Global averages

We begin our study by analyzing the global average of the temperature in the troposphere, here defined as the average of the lowest 4 levels from the balloon radiosonde measurements (850 hPa – 300 hPa). Below, in Figure 3, we show the correlation between global tropospheric temperature anomalies and EUV radiation and galactic cosmic rays. In the top panels are shown the raw data giving correlations of 0.33 with EUV and –0.31 with GCR. In the temperature the effect of particularly the El Niño is clearly seen. In the middle panels the internal climate modulators, NINO3, NAO, and VAI have been removed from the temperature together with a linear trend by linear regression. A linear trend has also been removed from the GCR and EUV curves. The correlation coefficient grows somewhat to 0.42 and –0.47. The improved correlation is clearly seen by visual inspection. However, since all the external parameters are strongly modulated by the solar cycle, it is not at all obvious how to distinguish coincidental correlation from actual physical influence. In the bottom panel we have therefore removed the solar cycle, represented by the monthly sunspot number, from both the temperature and the external parameters. The correlation drops significantly, most dramatically for the EUV-temperature

correlation. In Table 3 we give the correlations for all 5 external parameter for raw data, with NINO3, NAO, VAI, and a linear trend removed, and with the solar cycle removed. The numbers in parentheses are the same correlation coefficients but after a 3 months box average has been applied. Particularly, TSI, EUV, and GCR show strong correlations. However, these correlations drop significantly after removal of the solar cycle. Only the GCR correlation survives to some extent.

One must bear in mind that the correlations for the various parameters are not calculated over the same time period. TSI and HPI are only available from November 1978. In Table 4 we show the correlations if we limit the analysis for all the parameters to this period. The correlations for UV, SW, GCR, and SSN drop. In fact, only the correlations for UV and SSN are above the 95% significance level after removal of the internal modes of variability. After removal of the solar cycle none of the parameters show any correlation.

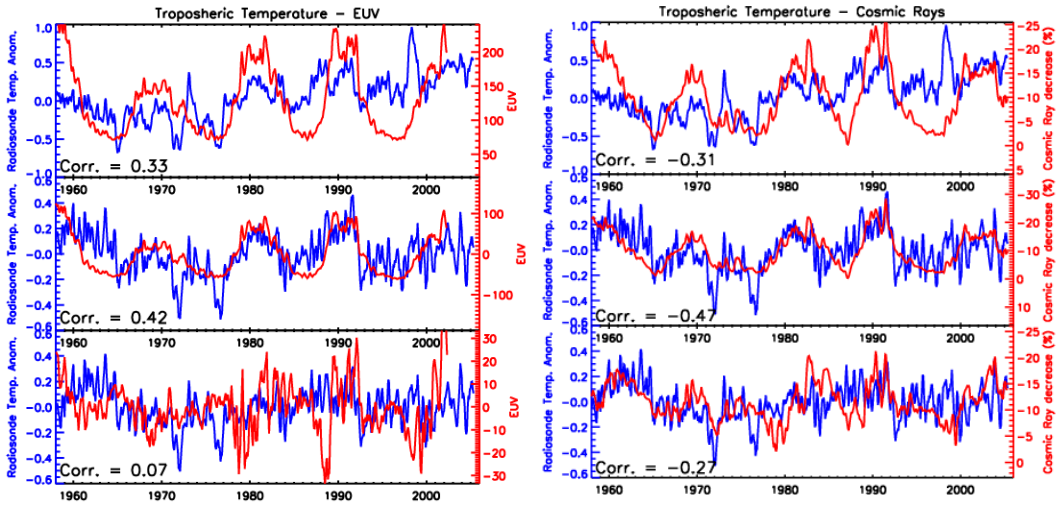

Figure 3: Left) correlation between 10.7 cm EUV proxy and global mean temperature anomalies for the troposphere. Top panel: observations. Middle panel: after removal of nino3, NAO, volcanic aerosols, and a linear trend. Bottom: after removal of the solar cycle. Right) the same for galactic cosmic rays.

	TSI	EUV	SW	HPI	GCR	SSN
Observ.	0.13 (0.16)	**0.33 (0.35)**	**0.20 (0.31)**	-0.08 (-0.07)	**-0.31 (-0.33)**	**0.25 (0.27)**
Niño, etc.	0.31 **(0.44)**	***0.42 (0.50)***	0.19 **(0.35)**	0.07 (0.14)	***-0.47 (-0.57)***	***0.40 (0.48)***
Solar cycle	0.05 (0.00)	0.07 (0.07)	-0.02 (0.02)	-0.01 (0.03)	**-0.27 (-0.33)**	

Table 3: the correlations coefficients for the 5 external parameters with tropospheric temperature. Given are the correlations for raw observation, after removal of the internal climate parameters, and after removal of the solar cycle. Numbers in bold face are above the 95% significance level. Numbers in bold italics are above the 99% significance level.

	TSI	UV	SW	HPI	GCR	SSN
Observ.	0.13 (0.16)	0.18 (0.21)	0.06 (0.08)	-0.08 (-0.07)	-0.16 (-0.18)	0.12 (0.14)
Niño, etc.	0.31 (0.44)	**0.39 (0.50)**	-0.13 (-0.23)	0.07 (0.14)	-0.22 (-0.27)	***0.42 (0.54)***
Solar cycle	0.05 (0.00)	0.04 (0.03)	-0.06 (-0.06)	-0.02 (0.03)	-0.05 (-0.04)	

Table 4: same as Table 3, but limited to the period November 1978-present.

Zonal averages

The various external parameters may influence different parts of the globe differently, both geographically and at different altitudes. Below we analyse the correlations with zonal averages of temperature anomalies given by balloon radiosonde measurements at nine different altitude levels (850 hPa – 30 hpa).

In Figure 4 we illustrate the analysis for the GCR parameter. For the raw observations (top, left) a clear correlation is seen in the troposphere, particularly strong in the tropical region, but without much signal in the stratosphere. After removal of the internal climate parameters (top right) the region of strong correlation extends into the stratosphere. However, after removal of the solar cycle (bottom, left) most of the correlations disappear. The correlation with the solar cycle (bottom, right) displays very much the same pattern as the GCR correlation before removal of he solar cycle. The zonal correlations with GCR are made for the full time period 1958-present. Limiting the analysis period to 1978-present will reduce the correlations corresponding to what is seen in Table 4.

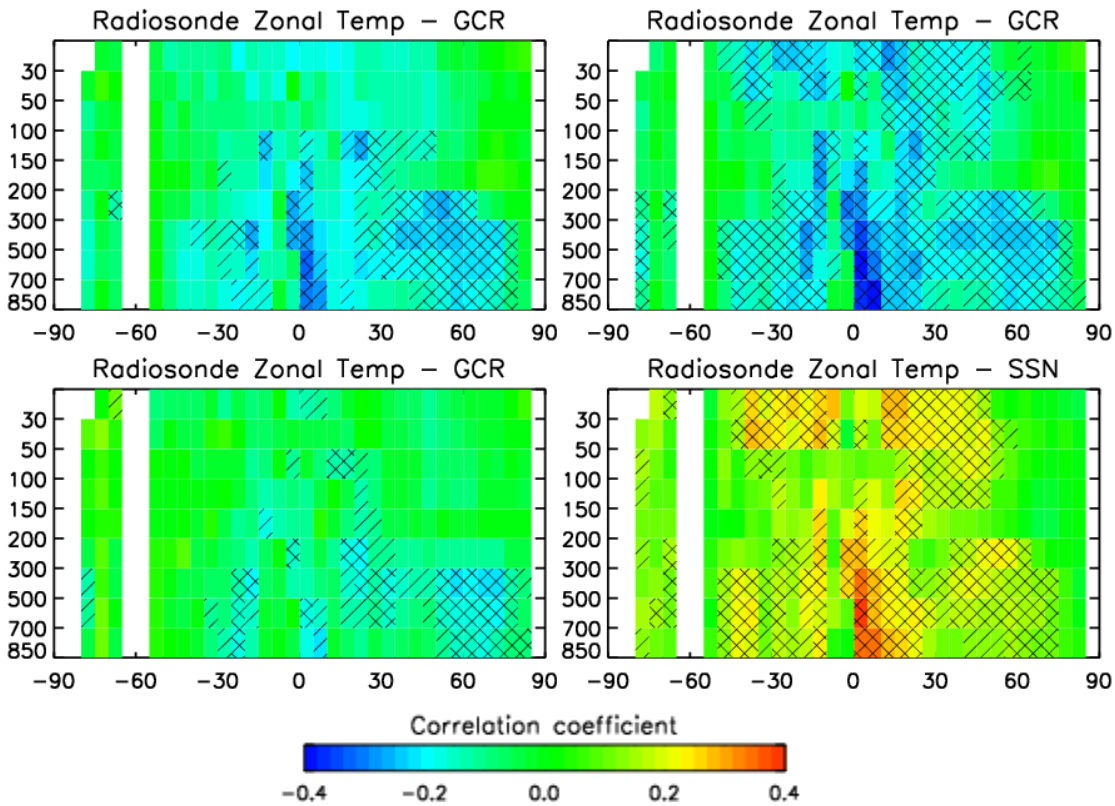

Figure 4: zonal correlations between GCR and radiosonde temperatures. Top left: raw observations. Top right: after removal of nino3, NAO, VAI , and linear trend by linear regression. Bottom left: after removal of the solar cycle. Bottom right: zonal correlation between sunspot number and radiosonde temperatures. Hatched areas have correlations above the 90% significance level, cross hatched above 95%.

Figure 5 shows the zonal temperature correlations with the external parameters after removal of the solar parameters. None of the parameters displays correlations comparable to those between temperature and sunspot number, though GCR and EUV do show some areas with significant correlations.

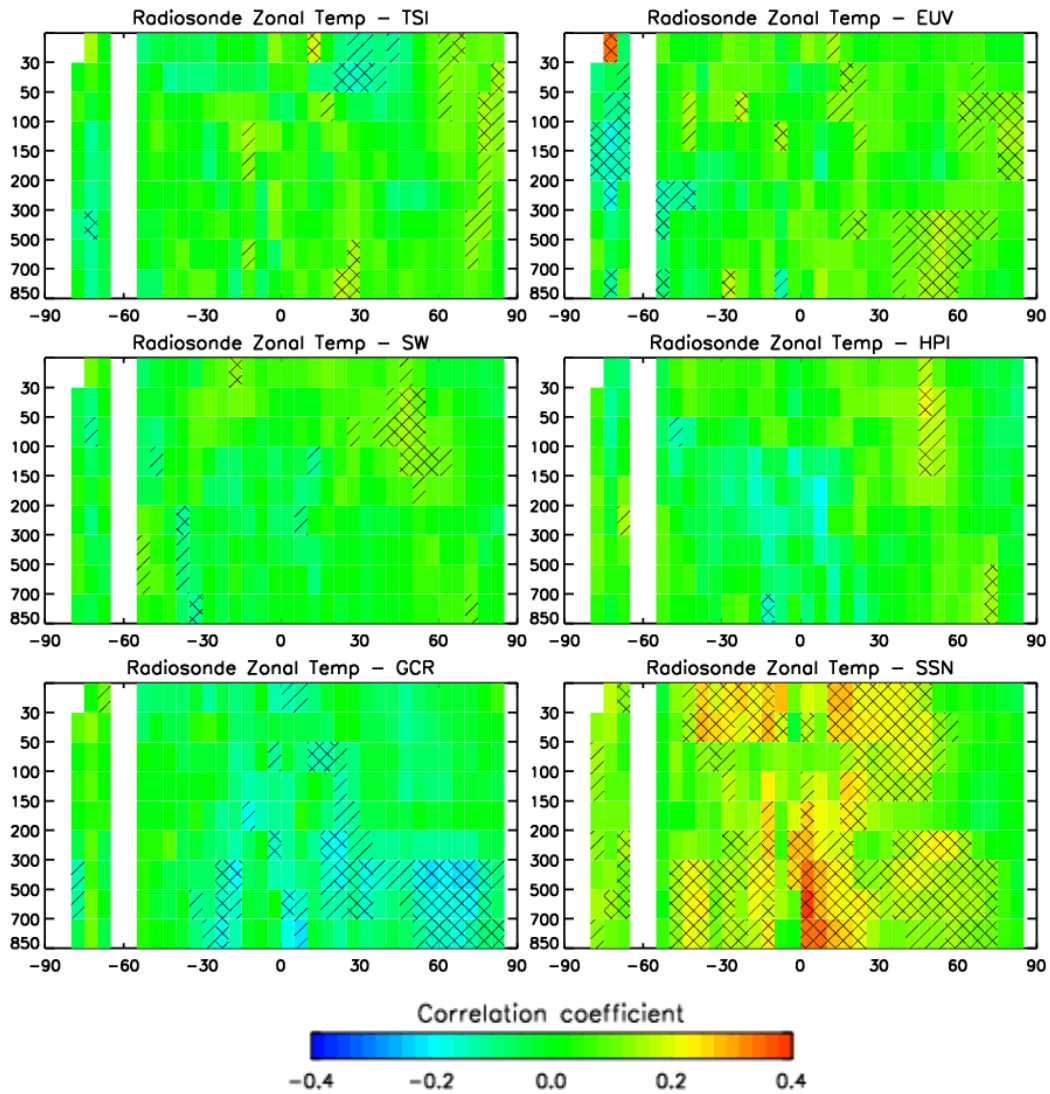

Figure 5: zonal correlations between the 5 external parameters plus the sunspot number and radiosonde temperature anomalies. The correlations are calculated after removal of the solar cycle. From top TSI and EUV, SW and HPI, GCR and SSN. Hatched areas have correlations coefficients above the 90% significance level, cross hatched above 95%.

MSU temperatures

Since the radiosonde temperature data are only collected over land, we use the MSU satellite measurements of temperature to show the geographical distribution of correlations between tropospheric temperatures and the solar modulated forcing parameter (Figure 6). Most notably, UV displays a band of positive correlation in the tropics, and HPI a band of negative correlations in the same region. GCR displays some negative correlations in the temperate and polar zones, while SSN various patches of mainly positive correlations. It should be noted that the MSU measurements only cover the period 1978-present.

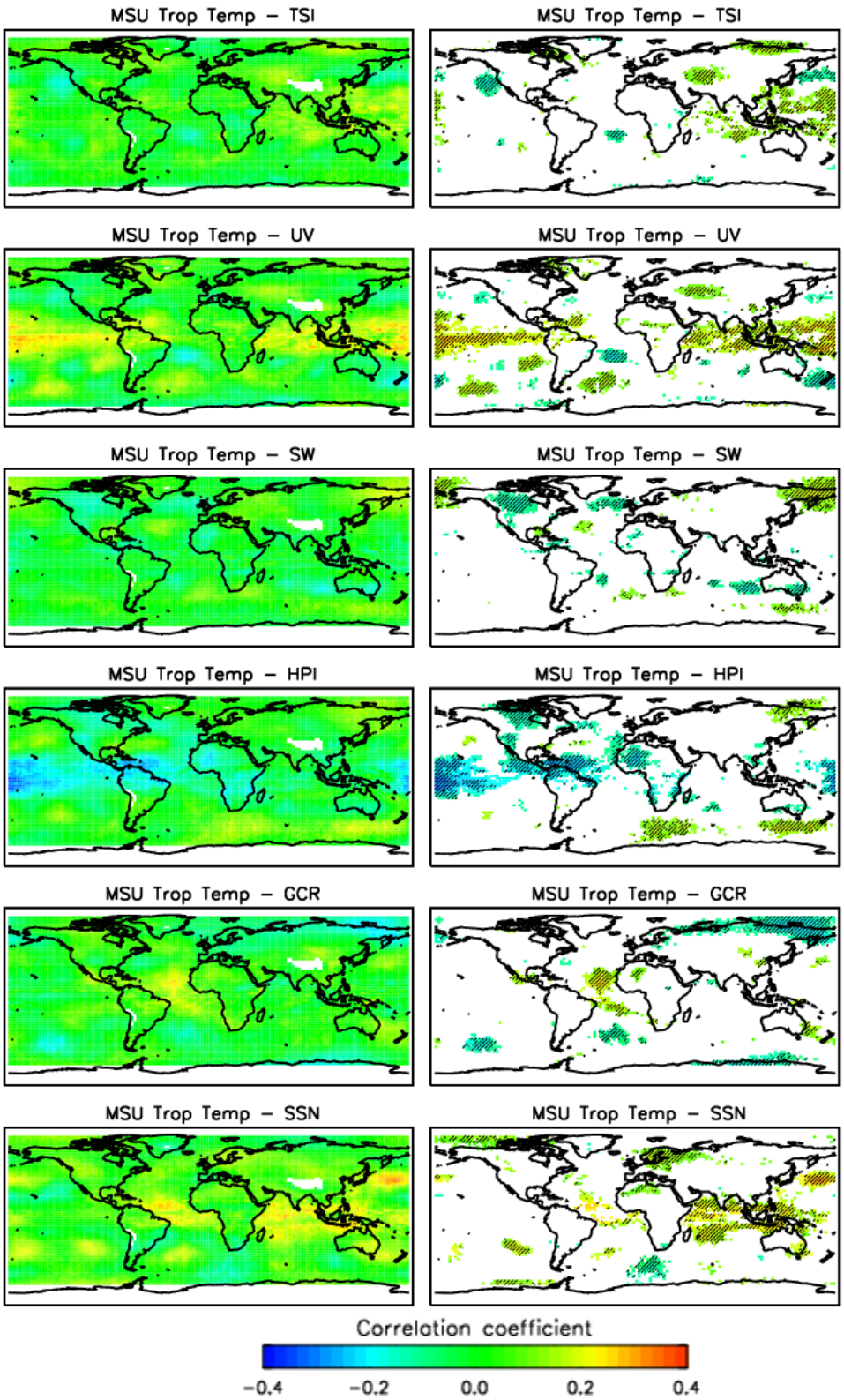

Figure 6: correlations between the 5 external parameters plus the sunspot number and tropospheric temperatures measured from satellite. The correlations are given after the removal of the internal parameters and the solar activity. To the right are shown only the areas with correlations coefficients above the 90% significance level, hatched areas are above 95% significance.

Conclusions for temperature correlations

Key results for each of the solar modulated forcing parameters are:

TSI: correlates reasonably well with tropospheric global mean temperature with a correlation coefficient of 0.31, 0.44 when smoothed over 3 months. This correlation, however, disappears after the solar cycle is removed from both temperature and TSI. In the zonal averages very little is seen. Geographically, a patch of positive correlation is seen in the western Pacific.
UV: the second strongest correlation for global mean temperature, the strongest (and only one above 95% significance level) when limiting the time period to 1978-present. Geographically, UV shows a band of positive correlation in the tropics.
SW: moderately correlated with global mean temperature. Geographically, the correlations mainly fall in the temperate and polar zones in the northern hemisphere.
HPI: does not correlate well with global mean temperature, though geographically it does show patches of negative correlations in the tropics.
GCR: strongest correlation with global mean temperature. The only parameter where the correlation survives removal of the solar cycle. Zonally, the correlations are strongest in the lower troposphere on the northern hemisphere.
SSN: carries almost all the correlation of the other parameters. The correlations are strongest in the tropics and extends through both troposphere and stratosphere.

The main features are:

- The solar cycle represented by the sun spot number is responsible for the major part of the correlations between temperatures and the solar modulated forcing parameters. Taking out the solar cycle from the signals removes most of the correlations.
- GCR is the only parameter with a moderately strong correlation (0.27) with the global mean temperature after removal of the solar cycle.
- UV shows correlations comparable to those with GCR, but they disappear after removal of the solar cycle.
- Limiting the time period to 1978-present lowers the correlations of particularly GCR.
- Geographically, the correlations are highest in the tropics when viewed over all 5 parameters.

Solar max/min

The previous section describes how the solar parameters are correlated with tropospheric temperatures over the past 45 years. In this section the correlation between the Hadley radiosonde temperatures and the 5 solar modulated parameters are investigated during periods of solar minimum and solar maximum. The aim is to analyze the short term fluctuations and identify any differences in the correlation properties over these respective periods.

Data period

The Hadley temperatures (HADAT) are available during 1958-2005; however, the analysis is limited by availability of the solar modulated parameters. Since reconstructions of solar activity based on sunspot number etc. are not used in this study, the analysis is limited to the period of direct observations beginning in 1963 for the three variables EUV, GCR and SW, and from 1978 for all five variables TSI, UV, GCR, SW, and HPI.

The solar max/min period for a solar cycle was chosen as the time period where the sunspot number is greater/smaller than the mean sun spot number. The mean sunspot number was calculated separately for each of the 4 solar cycle periods. This method provides both good statistics from the monthly averages and prevents any overlapping between consecutive min/max conditions. Figure 7 is a repeat of Figure 1f but with the periods used for analysis around solar min and solar max indicated by colors. To illustrate how fluctuations occur during a solar max period compared to a solar min period a smooth function has been subtracted from the sun spot number data in the bottom of Figure 7. Here it can be seen that the fluctuations in solar activity are greater under solar max conditions than under solar min conditions. TSI and HPI are only available from late 1978 hence the beginning of the solar max period under solar cycle 21 has been delayed. This is indicated by the gap in selected data in the lower panel of figure 7.

The following time periods of solar min and solar max were used for the analysis. The colours indicate which parameters described above are available over the different periods.

Solar Max: 1966-1973, 1978-1983, 1988-1993, 1998-2002
Solar min: 1963-1966, 1973-1978, 1983-1988, 1993-1998

The internal modes of variability have been removed from the HADAT data, and a mean, trend, and solar cycle have been removed from both HADAT and the solar modulated parameters using the multiple regression method described in the section Analysis Method.

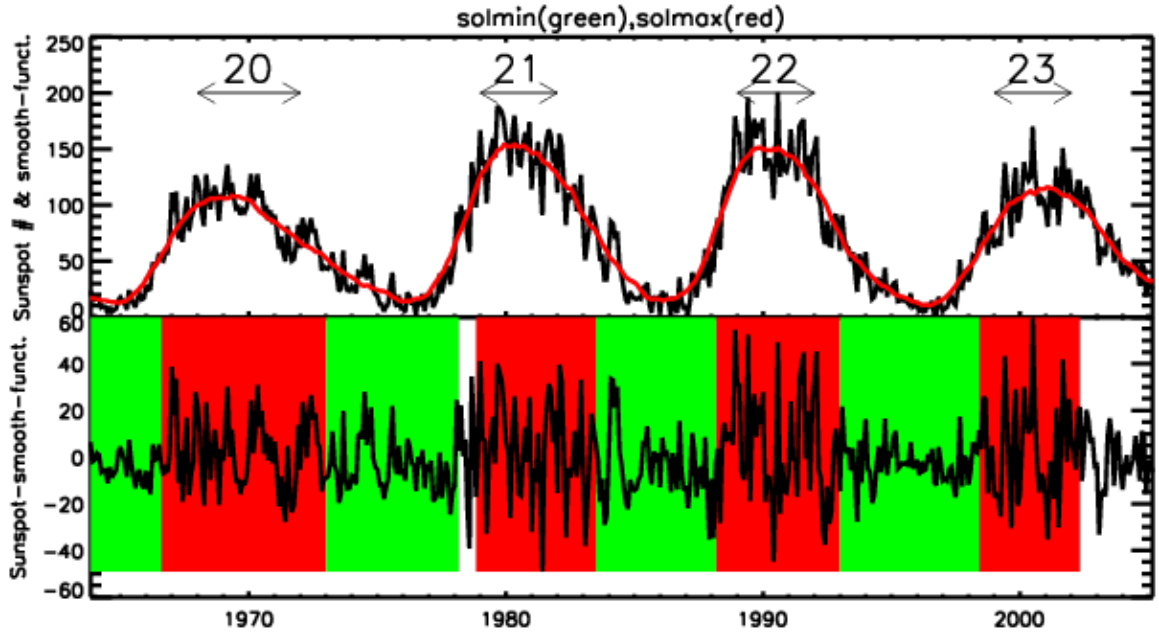

Figure 7: Top: sun spot number with smooth curve. Bottom: sun spot number with smooth curve subtracted. Solar min/max periods are defined by means of individual solar cycle periods. solar min (green) and max (red) .

Analysis under Solar min and Solar max conditions

The following sections describe the results of the correlation analysis performed between HADAT data and each of the five solar modulated parameters.

GCR

Figure 8 shows a plot of the correlation coefficients of solar max and min periods for the GCR signal with HADAT zonal anomalies covering three different time periods: 1963-1978, 1978-2002 and 1963-2002.

Over equatorial regions during the solar max of 1968-1971 a negative correlation is found in the troposphere up until 150 hPa, which switches to a positive correlation above 150 hPa in the stratosphere. There is little or no significant correlation outside of 30º in either hemisphere.

From 1978 onwards a significant correlation pattern is found in the troposphere which is negative under solar max conditions and positive under solar min conditions. This correlation pattern persists throughout the whole period of available observations, and is largely restricted to ±30º latitude up until 100 hPa. Under solar max conditions there is an additional significant negative correlation around 60ºN near the surface.

The change in sign of the correlation between solar min and solar appears to be robust. However, it is an unusual feature since it suggests that if the temperatures are really responding to GCR then the nature of the response can be quite different during different phases of the solar cycle.

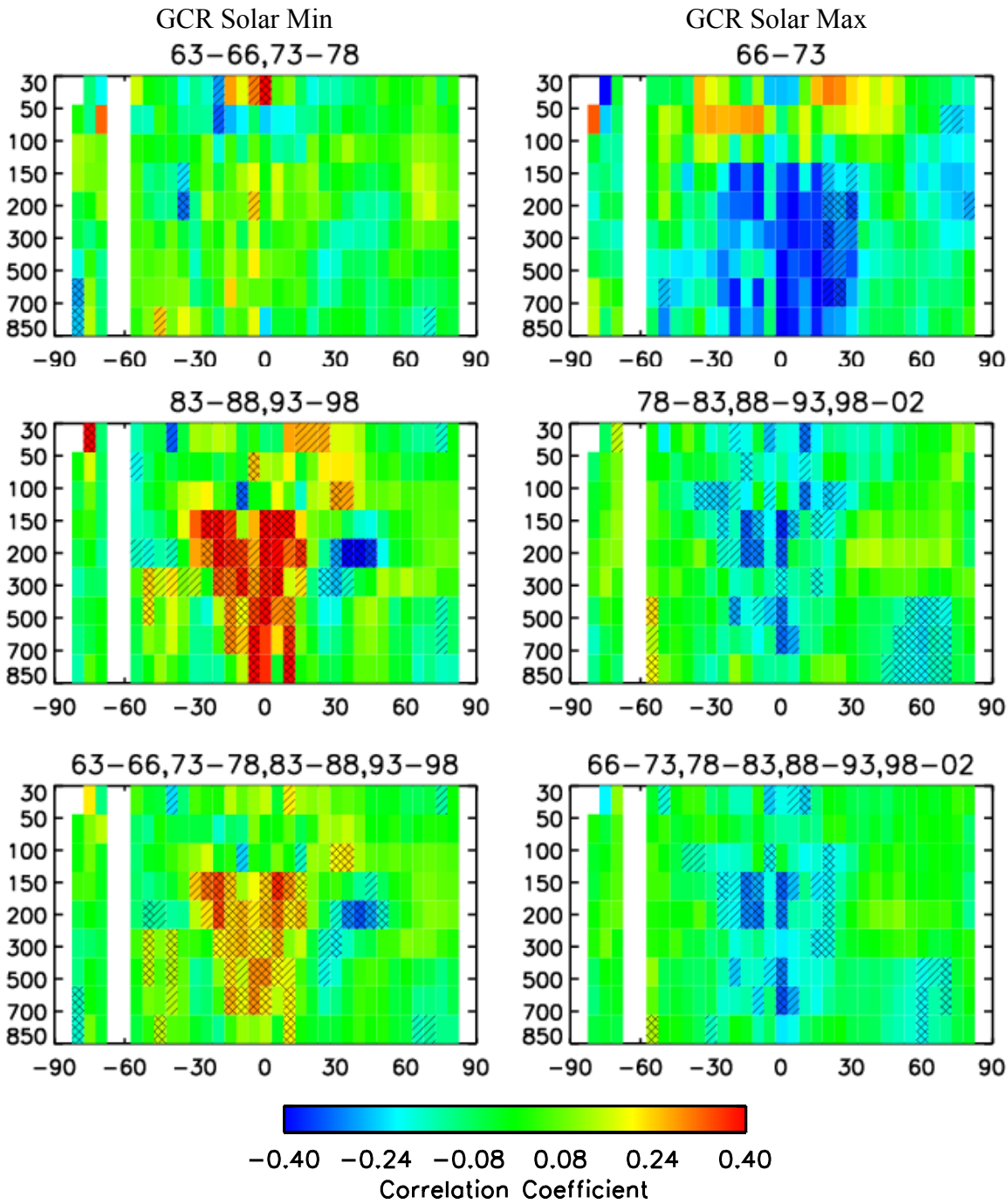

Figure 8: Plot of correlation coefficients of GCR signal with Hadley zonal anomalies. 3 different time periods are shown. Correlations with significances higher than 0.9 and 0.95 are hatched and cross hatched, respectively.

UV

Figure 9 shows a plot of the correlation coefficients of solar max and min periods for the EUV signal with Hadley zonal anomalies for three different time period: 1963-1978, 1978-2002 and 1963-2002.

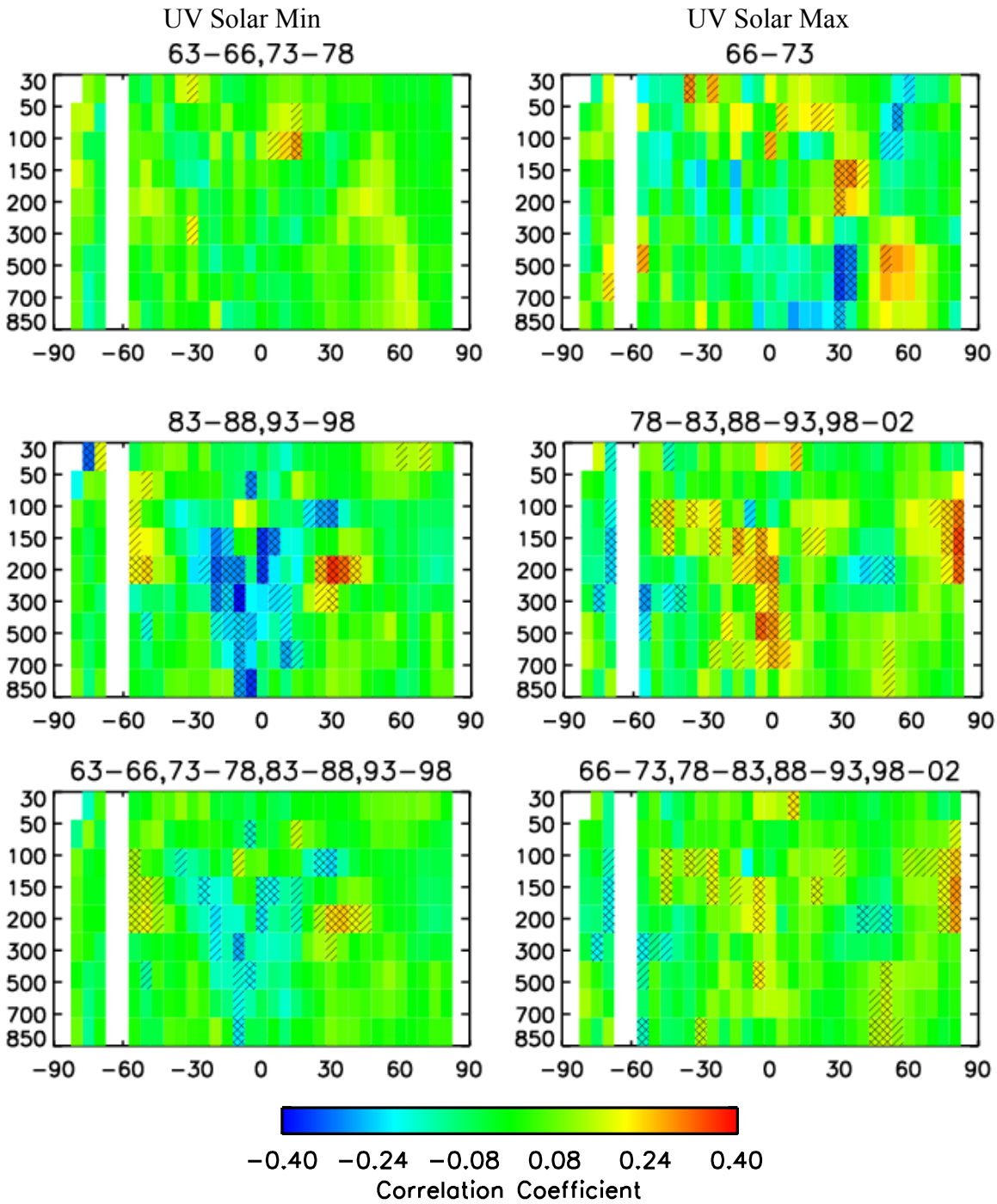

Figure 9: Plot of correlation coefficients of UV signal with Hadley zonal anomalies. 3 different time periods are shown. Correlations with significances higher than 0.9 and 0.95 are hatched and cross hatched, respectively

The patterns are less clear here than for GCR. Prior to 1978 under solar max conditions there are a few areas of both positive and negative correlation in the northern hemisphere. During solar min conditions there is little correlation.

From 1978 onwards a similar correlation pattern to that seen with GCR, although much weaker and with a reverse in sign, is found in the troposphere under solar max/min conditions.

SW

Figure 10 shows a plot of the correlation coefficients of solar max and min periods for the SW signal with Hadley zonal anomalies for three different time periods: 1963-1978, 1978-2002 and 1963-2002.

Little significant correlation is found under solar max conditions. There is a negative signal in the mid-upper troposphere between the years 1978-2002, but this disappears when including all periods under solar max conditions from 1968-2002.

Solar min conditions show a significant negative correlation for the period 1978-2002 in the upper troposphere/stratosphere around 60ºS. However, when both periods are combined virtually all significant correlations disappear.

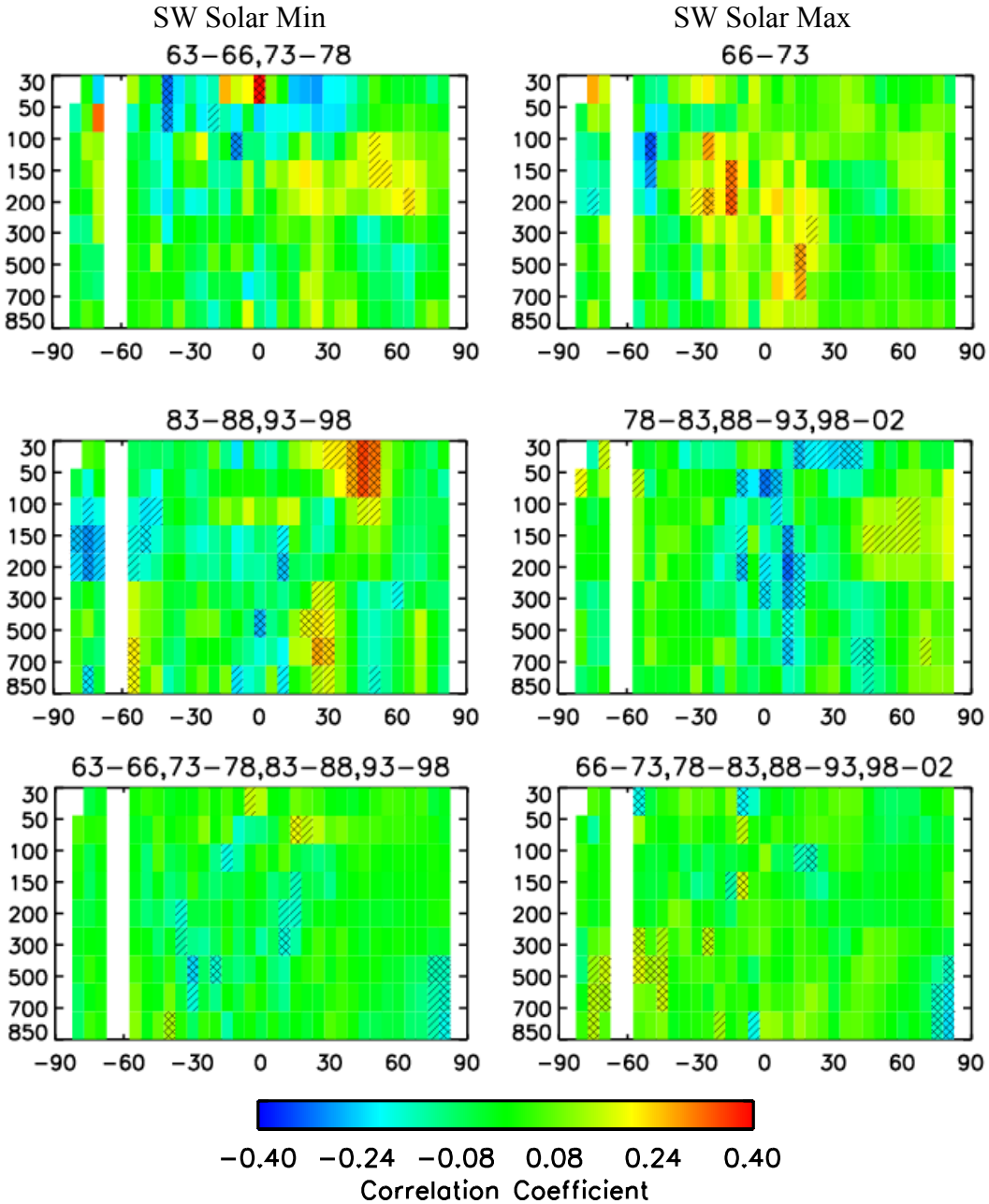

Figure 10: Plot of correlation coefficients of SW signal with Hadley zonal anomalies from 1978-2002. Correlations with significances higher than 0.9 and 0.95 are hatched and cross hatched, respectively

TSI

Figure 11 shows a plot of the correlation coefficients of solar max and min periods for the TSI signal with Hadley zonal anomalies over the time period where TSI data is available: 1978-2002.

In this period the correlation signal under solar min conditions is fairly weak, with the strongest significant correlation in the upper troposphere at high latitudes in the northern hemisphere.

During solar max there is a significant band of a weak positive correlation throughout the troposphere mostly around equatorial regions but also at higher latitudes.

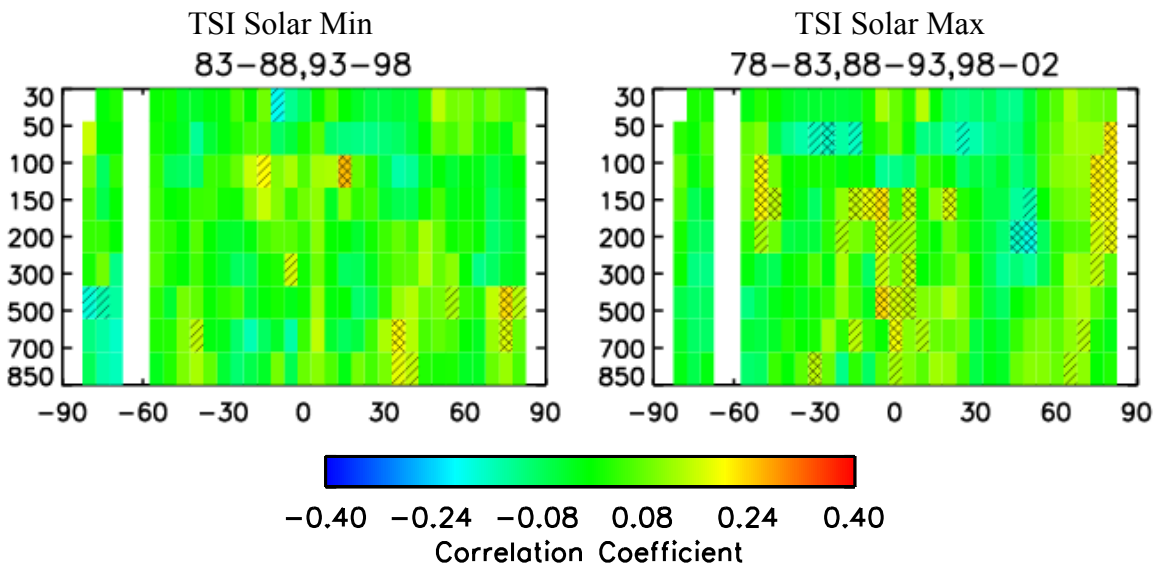

Figure 11: Plot of correlation coefficients of HPI signal with Hadley zonal anomalies from 1978-2002. Correlations with significances higher than 0.9 and 0.95 are hatched and cross hatched, respectively

HPI

Figure 12 shows a plot of the correlation coefficients of solar max and min periods for the HPI signal with Hadley zonal anomalies over the time period where HPI data is available: 1978-2002.

During solar max conditions some significant positive correlation appears in the stratosphere between 30ºS-30ºN and little elsewhere. However, under solar min conditions there is a significant negative signal throughout the troposphere around the equator.

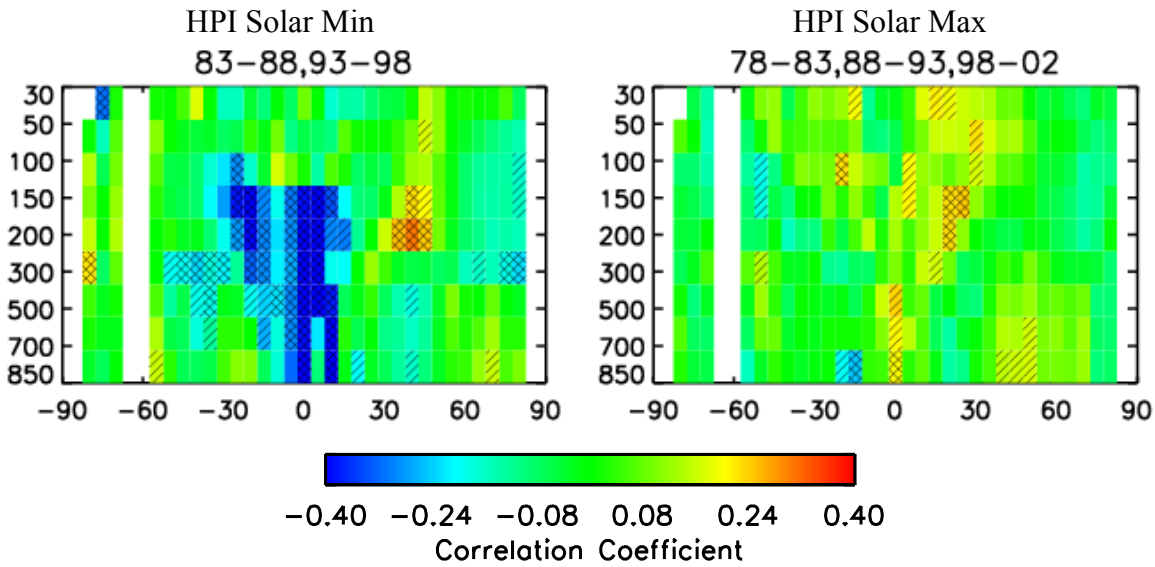

Figure 12: Plot of correlation coefficients of HPI signal with Hadley zonal anomalies from 1978-2002. Correlations with significances higher than 0.9 and 0.95 are hatched and cross hatched, respectively

Conclusions for solar min and max periods

The key results from this analysis under solar min and max conditions can be summed up for each of the solar modulated parameters as follows:

> **GCR:** A negative correlation is found in the troposphere under solar max conditions prior to 1978. After 1978 significant negative/positive correlation exists in the tropical troposphere under solar max/min conditions respectively after 1978.
> **UV:** Weak significant correlation structures of negative/positive correlation exist during solar max/min similar to those seen in GCR. Except for solar min conditions from 1963-1978 this structure is present over all periods.
> **SW:** Little significant correlations during solar max or solar min.
> **TSI:** Little significant correlation during solar min. During solar max a significant, but weak, band of positive correlation is found in the troposphere over the tropics.
> **HPI:** Little significant correlation during solar max. During solar min a significant band of negative correlation is found throughout the troposphere in the tropics.

The main features are:

- GCR shows a consistent negative/positive correlation under solar max/min conditions in the troposphere over the period 1978-2002. A similar pattern is seen with UV, but with a reversed sign and much weaker signal.
- Under solar min conditions SW, TSI, and HPI all display some significant correlations but with no common consistency between their sign or spatial distribution.
- HPI displays strong significant correlations during solar min.

Vertical Circulation

The NCEP remodelling project distributes a large number of meteorological parameters derived through a full 3-D physical model with assimilation of all available meteorological measurements from the period covered (1948-present). Here we focus on vertical circulation as an indicator of any possible shifts in the global climatological system. Figure 13 shows the correlation between vertical winds and the solar modulated forcing parameters.

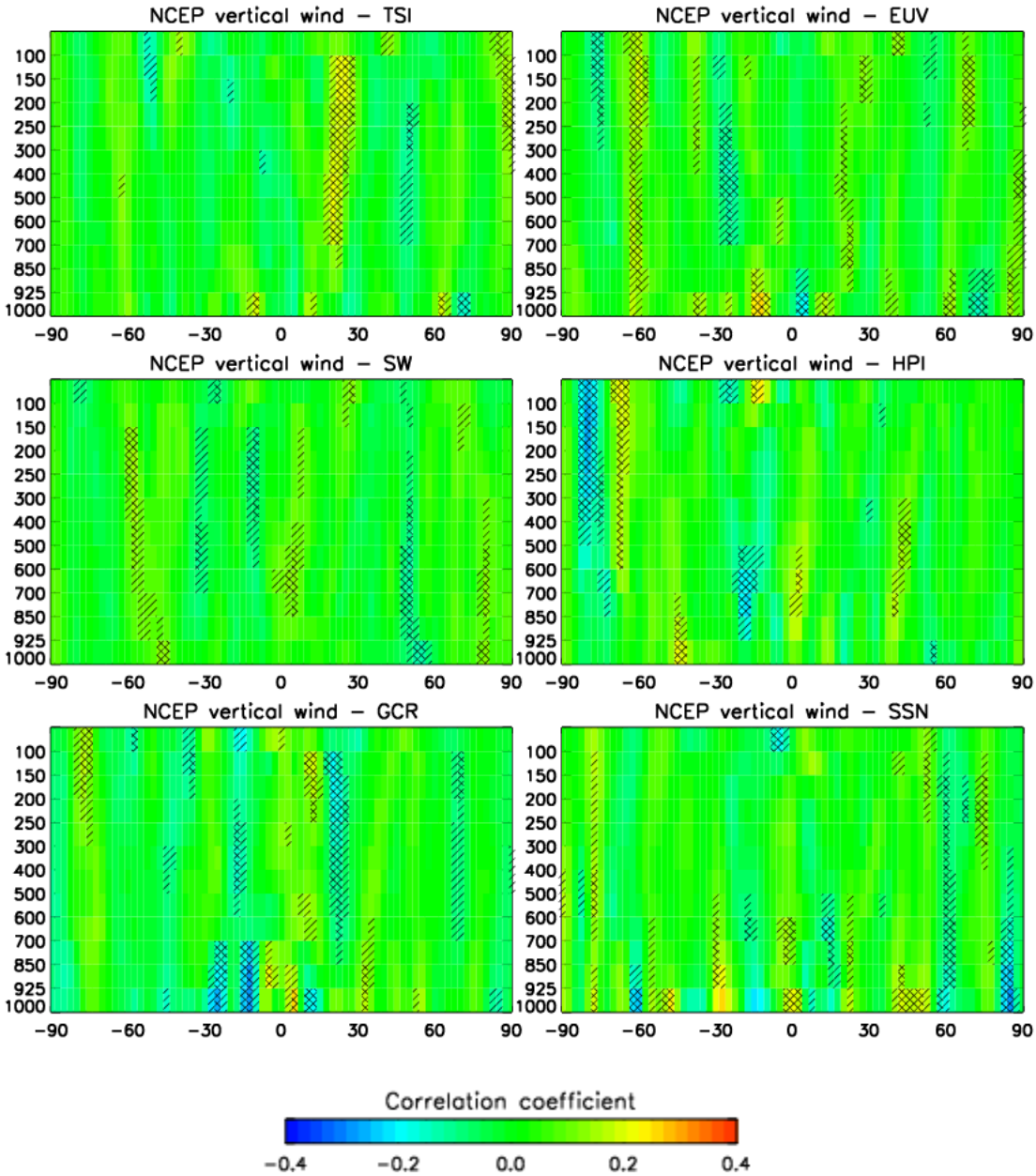

Figure 13: Correlations between vertical winds obtained from NCEP and the 5 external parameters plus the sunspot number. The correlations are calculated after removal of the internal modes of variability and the solar cycle.

All the parameters, including sunspot number, show latitudinal bands of alternating positive and negative correlations stretching from ground level in to the stratosphere,

though not positioned at the same latitudes for all the parameter. This points to a variation in the vertical circulation that varies on a number of time scales that coincides with the variation of the different external parameters at different latitudes. It is therefore not obvious that the co-variation of vertical circulation and the solar modulated forcing parameters should indicate a cause and effect relationship.

The main features are:

- All solar modulated forcing parameters show correlations in alternating positive and negative latitudinal bands stretching from ground level into the stratosphere.
- The correlations for the different parameters are very similar but not at the same latitudinal position.
- No clear conclusion can thus be reached for this climate parameter.

Low clouds

Low clouds are taken from the ISCCP cloud data sets which have recently been updated to provide a systematic view of global cloud behaviour over the period July 1983 – December 2004. ISCCP initially divides the clouds into three types based on altitude, low, middle, or high, using either infrared or a combination of infrared and visual observations. The analysis here is restricted to low clouds derived from infrared observations only.

Previous work has suggested that a problem with the continuous calibration exists at the end of 1994 and beginning of 1995. The problem is most easily noticed in the high cloud cover as demonstrated in Figure 14. A clear drop of more than 1% in global high cloud coverage is seen at the end of 1994. At the end of 2001 the high cloud coverage comes back up to the level pre-1995. Comparison with an independent data set of low cloud provided by the SSM/I microwave instrument aboard the DMSP satellites suggest that there is an offset between these two data sets. Following the procedure of Marsh and Svensmark (2003) the ISCCP low cloud data has been adjusted to account for this offset at every grid point after 1994. Below the analysis from both the original and adjusted data is presented.

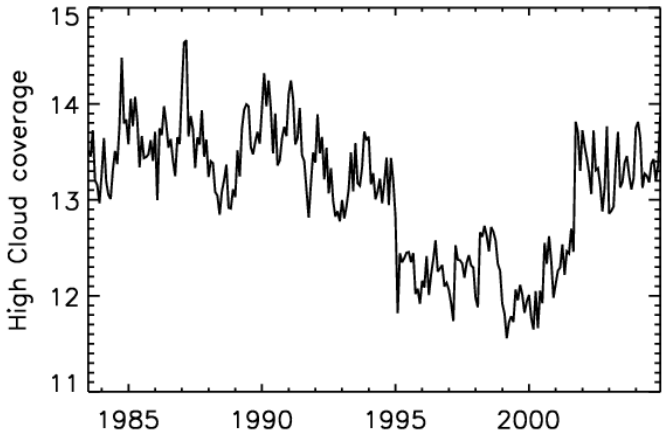

Figure 14: Global high cloud coverage with annual cycle removed.

	TSI	UV	SW	HPI	GCR	SSN
Observ.	-0.40(-0.46)	**-0.58(-0.62)**	-0.24(-0.37)	-0.08(-0.11)	0.40(0.43)	-0.36(-0.40)
Niño, etc.	**-0.41(-0.50)**	***-0.50(-0.57)***	-0.24**(-0.42)**	**-0.31(-0.43)**	***0.52(0.61)***	-0.42(-0.50)
Solar cycle	**-0.21**(-0.24)	***-0.50(-0.60)***	-0.07(-0.17)	-0.18(-0.27)	**0.35(0.41)**	

Table 5: the correlations coefficients for the 5 external parameters and the sunspot number with low cloud coverage. Given are the correlations for raw observation, after removal of the internal mode of variability, and after removal of the solar cycle. Numbers in bold face are above the 95% significance level, numbers in bold italics above the 99% significance level.

	TSI	UV	SW	HPI	GCR	SSN
Observ.	**-0.54(-0.67)**	**-0.61(-0.71)**	**-0.34*(-0.57)***	-0.30**(-0.40)**	**0.62(0.72)**	-0.57(-0.68)
Niño, etc.	-0.49**(-0.63)**	**-0.57(-0.68)**	-0.27**(-0.49)**	-0.28**(-0.39)**	***0.59(0.71)***	**-0.54(-0.67)**
Solar cycle	**-0.23**(-0.26)	***-0.41(-0.47)***	-0.03(-0.13)	-0.10(-0.17)	***0.32*(0.39)**	

Table 6: same as Table 5, but after adjustment with the SSM/I DMSP cloud data.

Tables 5 and 6 report the correlation coefficients between all 5 solar modulated parameters and low clouds (original and adjusted respectively). A key feature is that the strongest significant correlations are found with UV and GCR, both with and without the inclusion of the solar cycle. For the original observed data in Table 5 UV displays the strongest correlation, however, after filtering out internal climate modes GCR becomes slightly stronger. For the adjusted data in Table 6 correlation coefficients with GCR are actually slightly stronger than UV for both the observed and filtered data. The strong correlation with SSN indicates that a large fraction of these strong correlations are due to the solar cycle, however, a significant correlation still exists in UV and GCR once the solar cycle is removed. This displays the most consistent feature since both in the original and adjusted data it is the UV that possesses the strongest significant correlation.

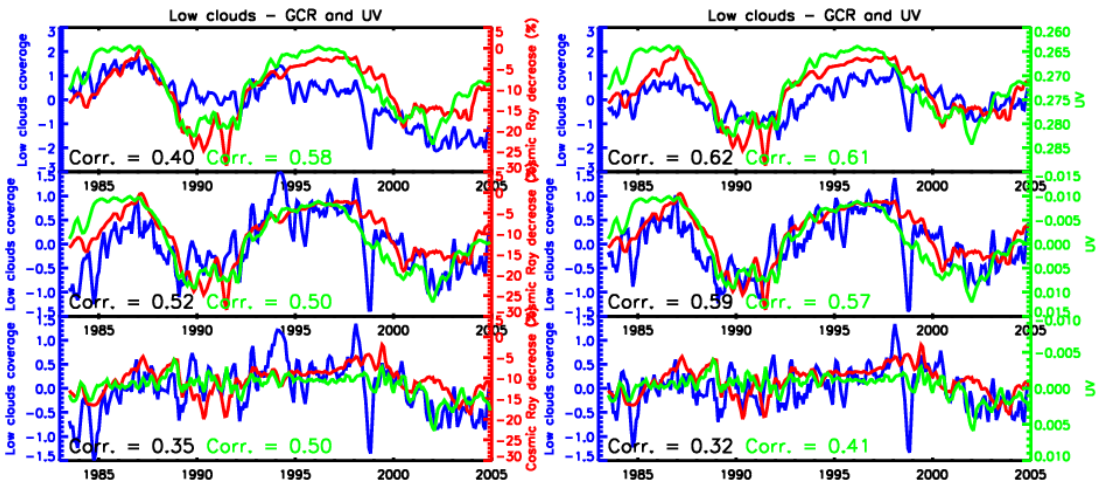

Figure 15: Correlation between GCR (red) and UV (green) and coverage of low clouds (blue). Left: ISCCP data for coverage of low altitude clouds. From top: annual cycle removed, trend and internal modes removed, solar cycle removed. Right: same as left, but after adjustment with the SSM/I DMSP cloud data.

Figure 15 shows a plot of UV (green) and GCR (red) together with the original (left) and adjusted (right) globally averaged low cloud data (blue). The correlation over nearly two and a half solar cycles is quite striking, particularly once the internal climate modes have been filtered out. The spatial distribution of correlation coefficients once the solar cycle has been removed (Figure 16) indicate that the strongest significant correlations are found at mid to high latitudes for both UV (negative) and GCR (positive). However, there also exist regions of positive (UV) and negative (GCR) correlation around the equator, particularly for GCR, which are washed out when taking the global average

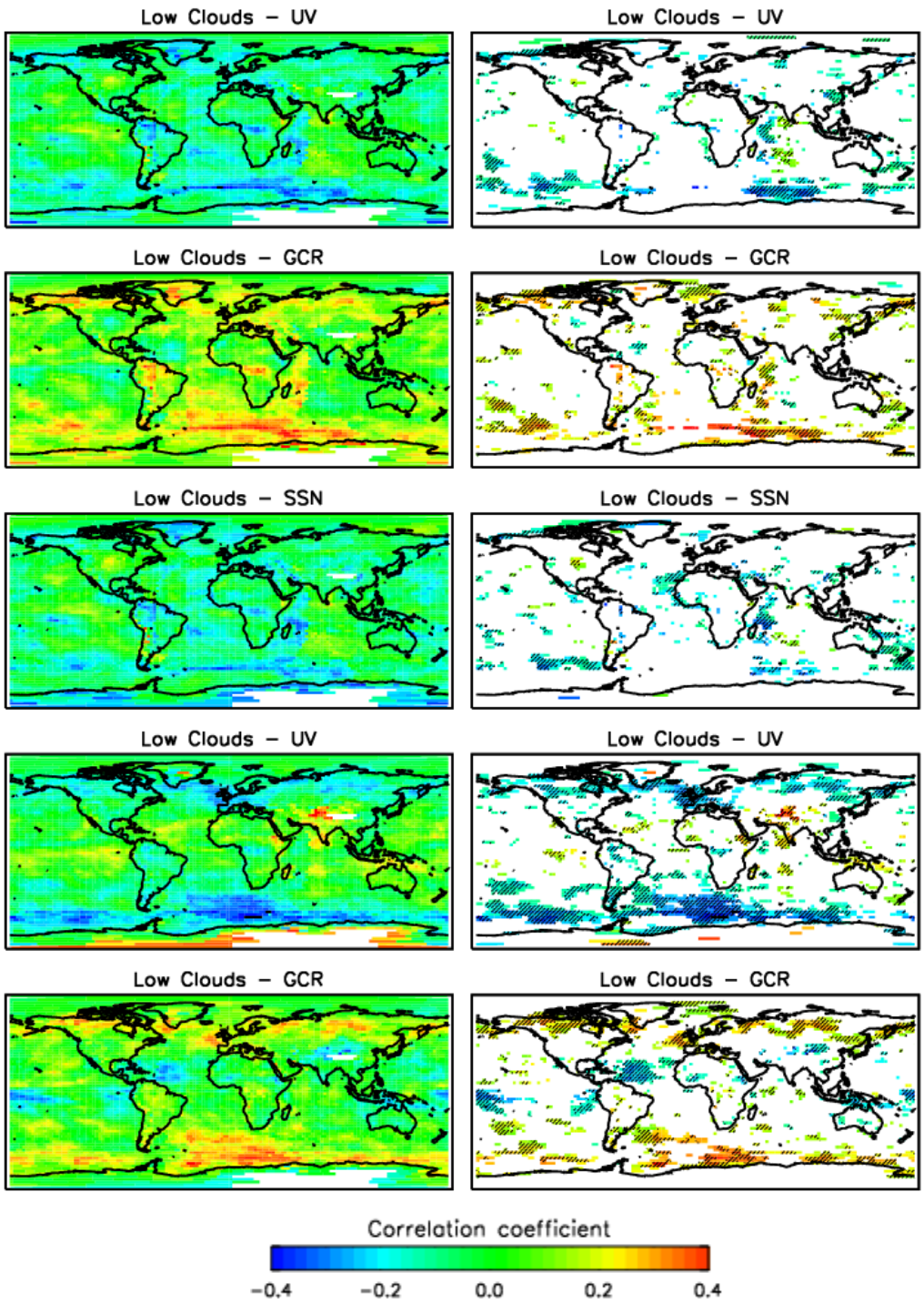

Figure 16: correlations between the UV and GCR plus the sunspot number and coverage of low clouds. The top two rows show the correlations with UV and GCR before the solar cycle is removed; third row shows the correlation with sunspot number; two bottom rows show the UV and GCR correlations after the solar cycle is removed. Some strong contrasts, for example in the Indian Ocean east of Africa are the effect of the foot point of the observing geo-stationary satellites. To the right are shown only the areas with correlations above the 90% significance level, hatched areas are above 95% significance.

We have concentrated on the correlations between low clouds and UV and GCR since these show the most prominent features. The key results are:

Calibration: a problem may exist with the continuous calibration of the ISCCP cloud data. We adjust with the low cloud coverage after comparison

with the independent SSM/I DMSP data set for low clouds. Since no such independent data set exists for high and mid-altitude clouds we concentrate our analysis on low clouds.
UV: show negative correlations at mid to high latitudes. After removal of the solar cycle these bands are strengthened considerably. Also a band of positive correlations arises in the tropics.
GCR: correlation signal opposite to UV with bands of positive correlations at mid to high latitudes. After removal of the solar cycle these bands are strengthened and a band of negative correlations is seen in the tropics.
SSN: mostly negative correlations with low cloud coverage spread over the entire globe.
TSI: negatively correlated with low clouds. Some of this correlation survives the removal of the solar cycle.
SW and HPI: negatively correlated with low clouds, but very little of this correlation survives the removal of the solar cycle.

The main features are:

- The solar cycle is negatively correlated with low clouds over most of the globe and is responsible for most of the correlation seen in SW, HPI, and TSI.
- UV and GCR show negative(positive) bands of correlations at mid to high latitudes. These bands are *strengthened* by removal of the solar cycle which also causes positive(negative) bands of correlation to appear in the tropics.
- UV and GCR display very similar behaviour and the effect of these two parameters is therefore hard to distinguish from each other.

Ozone

The Ozone data set used in this analysis is total ozone column (Dobson units) obtained from the Total Ozone Mapping Spectrometer flown on NASA's Nimbus-7, Meteor 3, and Earth Probe satellites covering November 1978-present. The data set is on a 1.25x1 degree data grid, see WP 202.

In Table 7 the global correlations between the solar modulated forcing parameters and ozone are listed. The solar cycle is responsible for most of the correlations though some of the correlations survive for UV and to a smaller extent for GCR and TSI

Figure 17 shows the geographical distribution of the correlations between the solar modulated forcing parameters after removal of the solar cycle, the sunspot number and total ozone column. Almost all the correlation lies in the solar cycle, represented by the sunspot number, with the correlations concentrated in two symmetric bands around the equator.

	TSI	UV	SW	HPI	GCR	SSN
Niño, etc.	***0.45***	***0.56***	0.29	0.14	**-0.52**	**0.48**
Solar cycle	0.15	**0.25**	0.03	0.08	-0.20	

Table 7: Global correlations for ozone after removal of the internal modes of variability and after removal of the solar cycle. Correlations in bold face are above the 95% significance level, bold italics above the 99% level.

The key results for each of the solar modulated parameters are:

TSI: some correlations in the northern hemisphere survive the removal of the solar cycle.
UV: bands of positive correlations in mid to high latitudes
SW: mainly negative correlations in the northern hemisphere.
HPI: very little correlation
GCR: Although a strong correlation is found in global averages, very little is seen in the spatial plots.
SSN: responsible for almost all the correlation between the solar parameters and ozone.

Main results are:

- Two strong symmetric bands of positive correlations are seen in the sunspot number around the equator.
- Only small amounts of correlations are observed for the solar modulated forcing parameters after removal of the solar cycle, but is stronger in the UV.

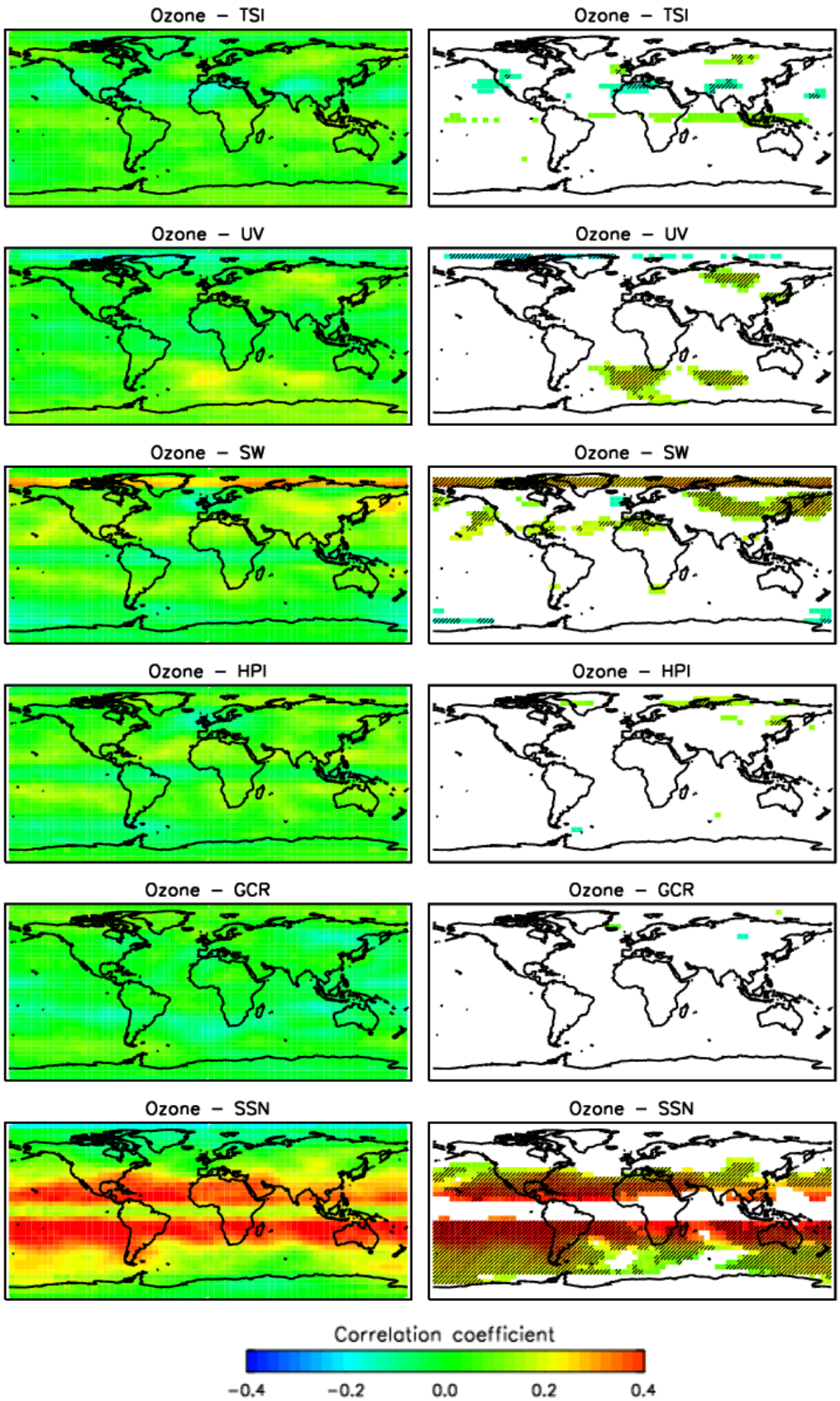

Figure 17: correlations between the 5 external parameters plus the sunspot number and total ozone column. The correlations are given after the removal of the internal parameters and the solar activity. To the right are shown only the areas with correlations above the 90% significance level, hatched areas are above 95% significance.

Aerosols

Aerosols have an effect on climate by altering the solar energy through absorption or scattering of solar radiation. Furthermore, aerosols can function as cloud condensation and freezing nuclei and thus play an indirect role in changing Earth radiation budget by altering the cloud formation and precipitation process.

The aerosol data index used in this analysis is from the TOMS instrument that delivers an aerosol index based on the absorption of an atmosphere containing aerosols compared to that of a pure molecular atmosphere. The aerosol index is positive for absorbing aerosols and negative for non-absorbing aerosols. The Aerosol index covers the period November 1978-present (See WP 202).

Table 8 lists the global correlations between the aerosol index and the solar modulated forcing parameters. It is worth noting that in this case the removal of the solar cycle increases the strength of correlation coefficient for UV, SW, and GCR, rather than removing their effect as with previous climate parameters. However, the strongest correlation is seen for the HPI parameter.

Figure 18 shows the geographic distributions of correlation coefficients between the aerosol index and the solar modulated forcing parameters. Strong correlation is observed for UV (positive correlation) and GCR (negative correlation) on the southern hemisphere. HPI shows strong correlations at the equator. In the case of the aerosol index there is almost no correlation with the sunspot number.

	TSI	UV	SW	HPI	GCR	SSN
Niño, etc.	-0.28	-0.13	0.05	**0.35**	0.03	-0.03
Solar cycle	**-0.19**	**0.19**	0.16	**0.37**	-0.26	

Table 8: global correlations between the solar parameters and the aerosol index after removal of the internal modes of variability and after removal of the solar cycle.

The key results for each parameter are:

TSI: very little correlation.
UV: strong positive correlations in the southern hemisphere.
SW: very little correlation.
HPI: strong positive correlations at the equator and some negative correlation at higher latitudes.
GCR: Strong negative correlations at low to mid latitudes in the southern hemisphere.
SSN: Almost no correlation

The main features are:

- Almost no correlation with the solar cycle.
- Strong correlations in the southern hemisphere for UV and GCR, and at the equator for HPI.

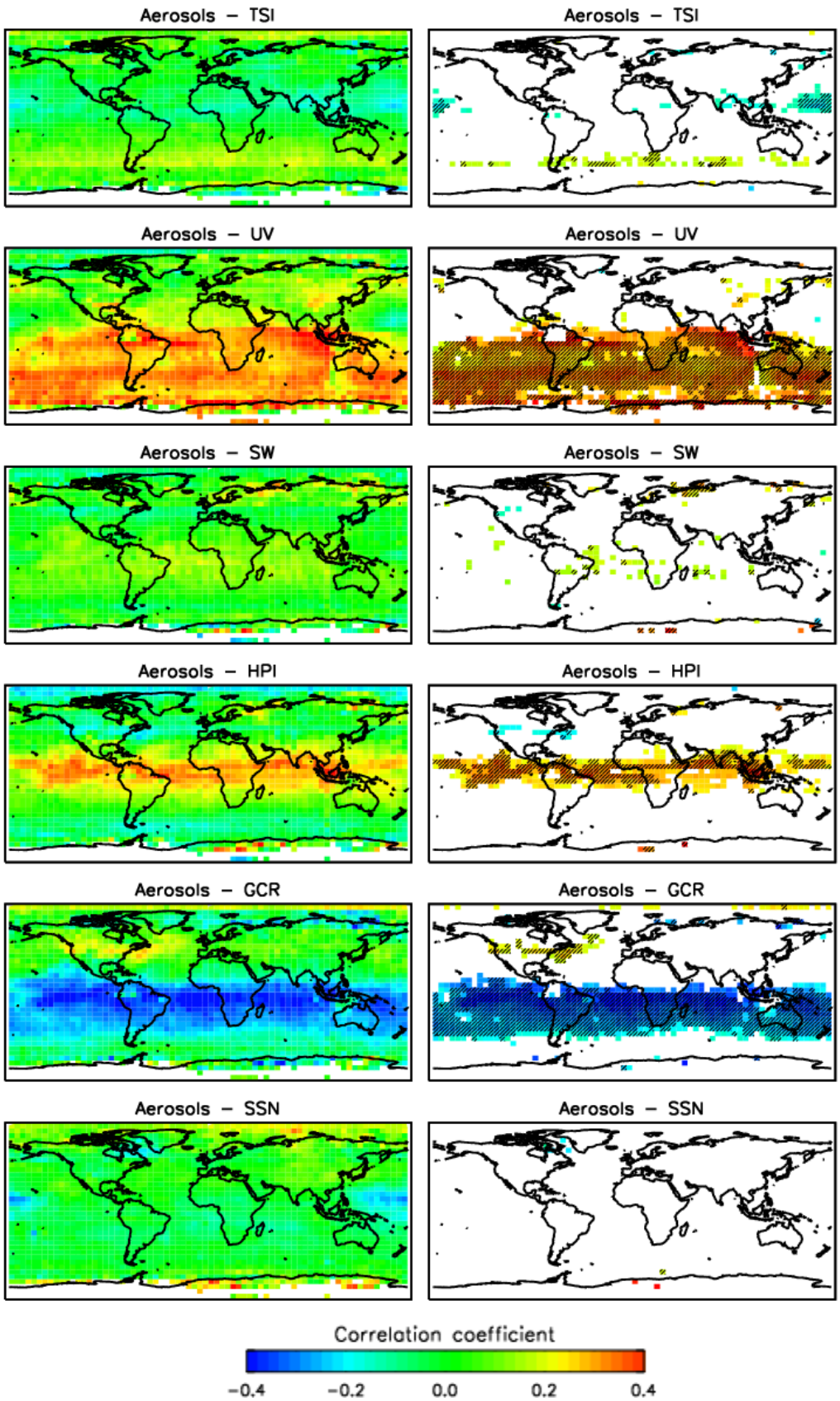

Figure 18: correlations between the 5 external parameters plus the sunspot number and the aerosol index. The correlations are given after the removal of the internal parameters and the solar activity. To the right are shown only the areas with correlations above the 90% significance level, hatched areas are above 95% significance.

Surface Response

The surface response to the solar parameters is investigated in this chapter. Focus is on how vegetation, snow, precipitation and surface pressure and temperature correlate with the solar parameters. Time series for selected areas are also shown.

Vegetation

NDVI is calculated from the visible (VIS) and near-infrared (NIR) light reflected by vegetation and expressed by: (NIR - VIS)/(NIR + VIS). Chlorophyll in healthy vegetation absorbs most of the visible light (for use in photosynthesis) and reflects a large portion of the near-infrared light. The NDVI value for healthy vegetation is thus close to 1. Unhealthy or sparse vegetation reflects more visible light and less near-infrared light and has a NDVI value closer to zero.

The NDVI index used in the analysis is computed from band measurements from the NOAA AVHR instrument. The data set is available from July 1981 to September 1994.
In Figure 20 we show the correlations between NDVI and the solar modulated forcing parameters. Only the correlations with more than 90% significance are shown. Basically very little is seen, except for a relatively strong correlation over central Europe for almost all the solar parameters. Due to the short period of availability of the NDVI index (1981-1994) the removal of the solar cycle does not make a large difference for this parameter. In Figure 19 we show the correlation between NDVI and UV and GCR over central Europe before and after removal of the solar cycle.

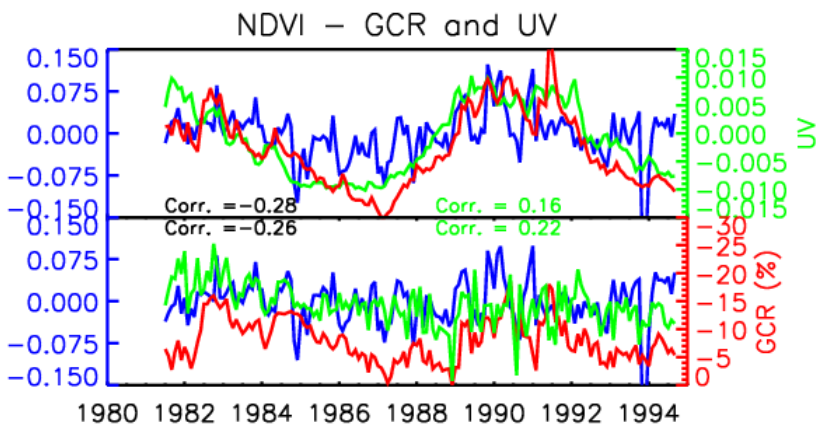

Figure 19: Correlation between NDVI and GCR and UV in central Europe (40-60° N, 0-50° E), before removal of the solar cycle (top) and after (bottom).

.

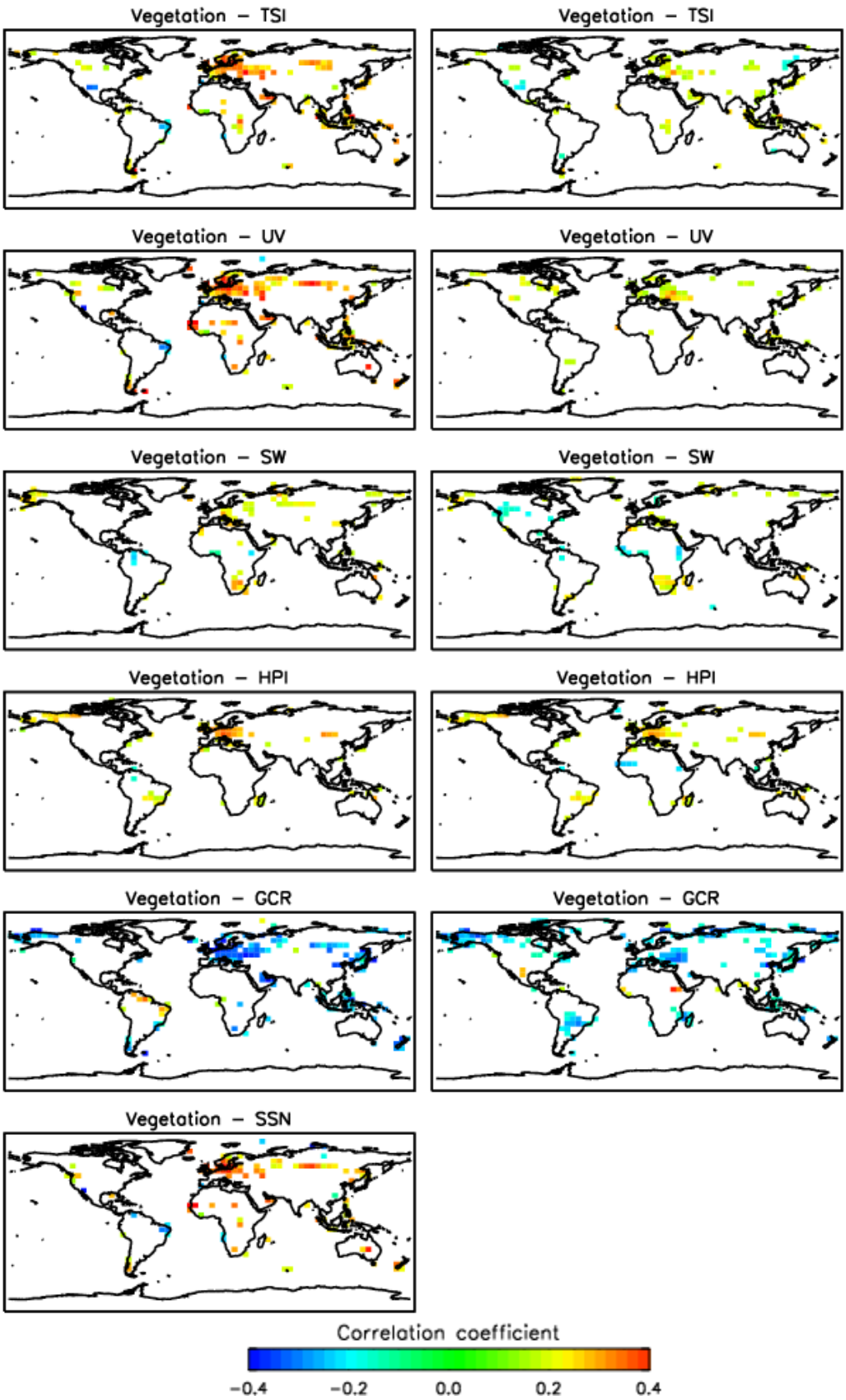

Figure 20: Correlations between the 5 external parameters plus the sunspot number and the normalized differenced vegetation index. The correlations are given after the removal of the internal parameters and linear trend (left column) and the solar activity (right column). Only the areas with correlation coefficients above the 90% significance level have been shown.

Snow

The snow data is monthly data from the Nimbus-7 SMMR Derived Global Snow Depth data set which is available from October 1978 – August 1987. The data is on a half-degree 720 by 360 lat/lon grid. Figure 23 shows the areas with correlations with significance above the 90% level. TSI seem to be somewhat negatively correlated and GCR somewhat positively correlated with snow depth. In Figure 21 we show the time series for snow depth for the areas with a significant positive GCR-correlation in North America together with the time series for GCR. Similarly, in Figure 22 we show the time series for snow depth for the areas with a significant negative TSI-correlation in Asia together with the time series for TSI.

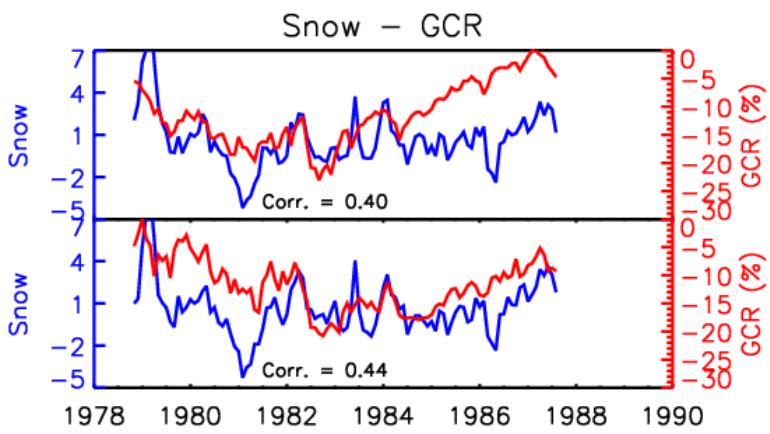

Figure 21: Correlation between snow depth and GCR in the areas of North America where the correlation is (significantly) positive (see Figure 23), before removal of the solar cycle (top) and after (bottom).

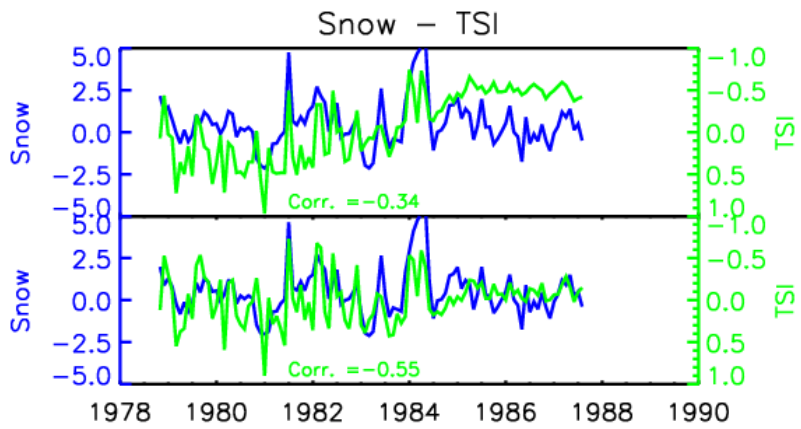

Figure 22: Correlation between snow depth and TSI in the areas of Asia where the correlation is (significantly) negative (see Figure 23), before removal of the solar cycle (top) and after (bottom).

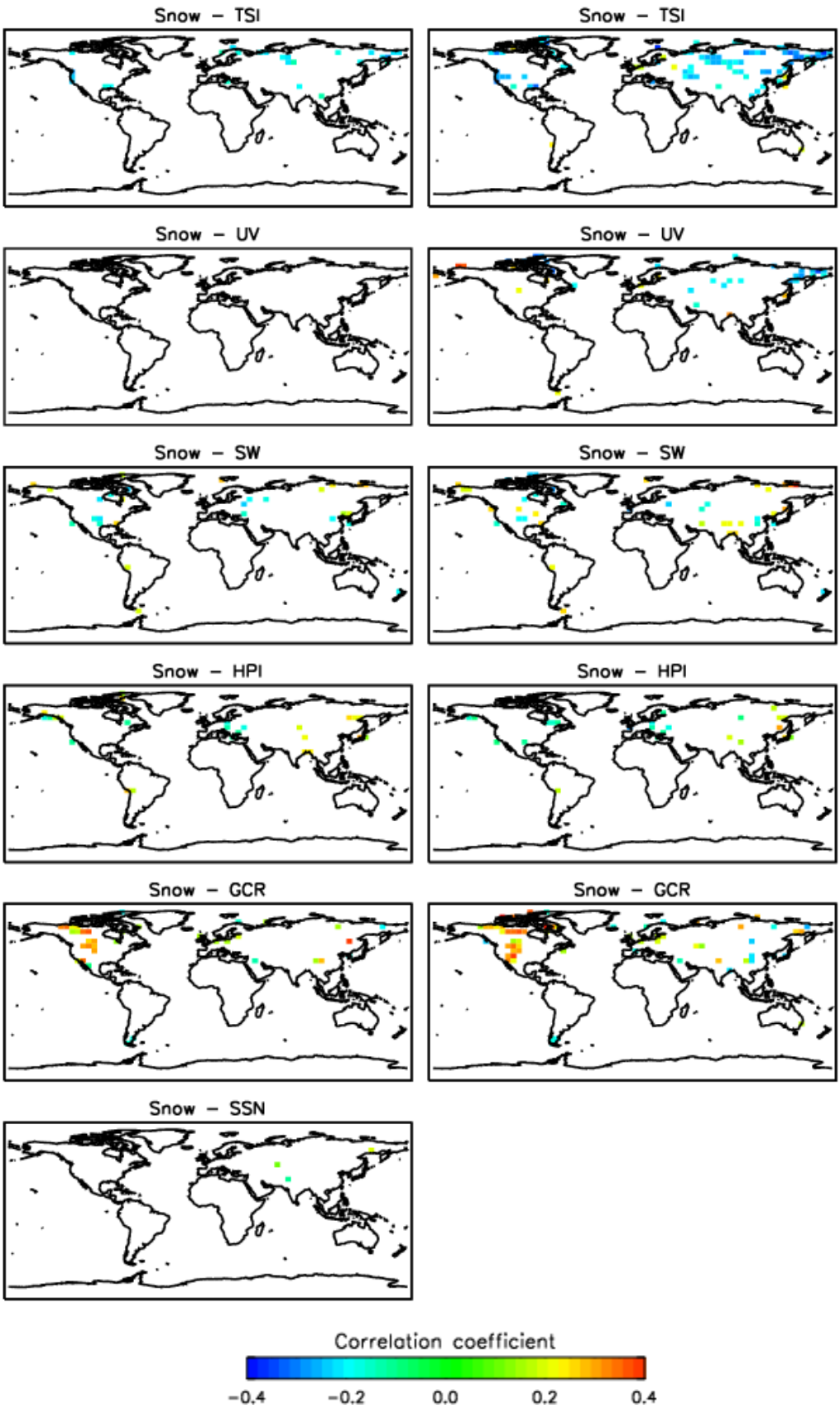

Figure 23: Correlations between the 5 external parameters plus the sunspot number and snow depth. The correlations are given after the removal of the internal parameters and linear trend (left column) and the solar activity (right column). Only areas with correlations above the 90% significance level have been plotted.

Sea Ice

The Sea Ice Extent is monthly data from the DMSP SSM/I instrument delivered by NCDC. The Sea Ice data are available from July 1987 – July 2005 on a 2.5° lat/lon grid. Figure 26 shows the areas with correlations with significance above the 90% level. GCR seems to be strongly correlated with sea ice close to the North pole and close to Antarctica, as does sunspot number. However, as can be seen in Figures 24 and 25, where we show the mean sea ice cover on the northern and southern hemisphere as derived from the SSM/I data, the strong correlation arises from an anomalous drop in the sea ice extent around 1991. This drop of nearly 10% of the sea ice cover must be suspected to be due to erroneous data.

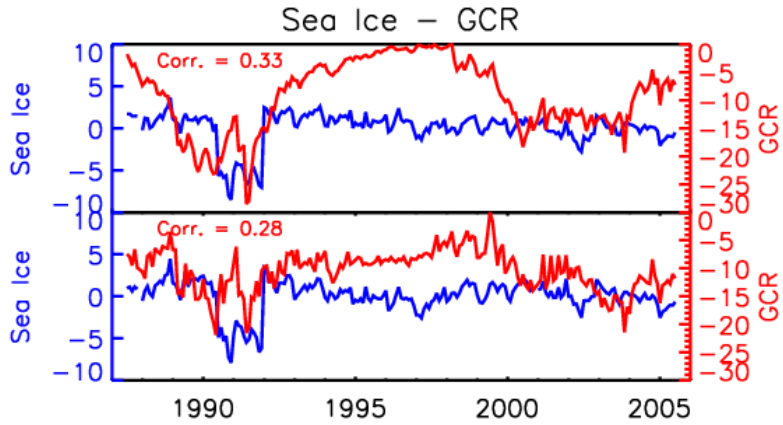

Figure 24: Sea Ice extent in the northern hemisphere above 45° after the removal of linear trend and internal modes of variability (top panel) and the solar cycle (bottom). The drop in sea ice cover around 1991 must be suspected to be due to erroneous data.

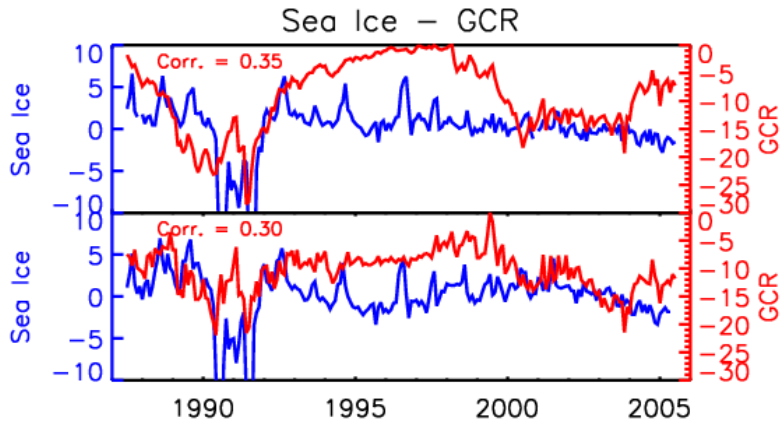

Figure 25: Equivalent to Figure 25, but for the southern hemisphere.

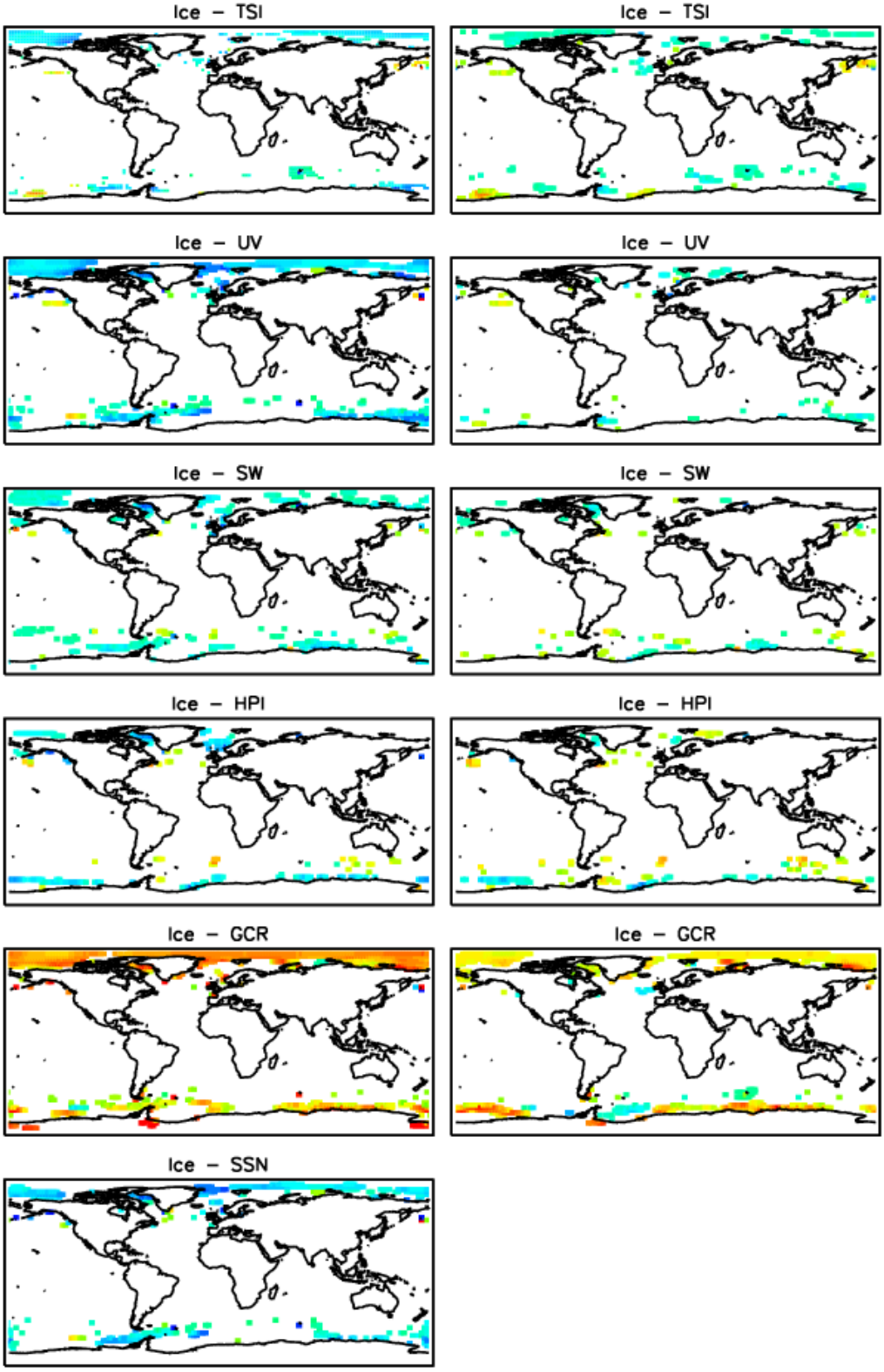

Figure 26: Correlations between the 5 external parameters plus the sunspot number and sea ice cover. The correlations are given after the removal of the internal parameters and linear trend (left column) and the solar activity (right column). Only the areas with correlation above the 90% significance level have been plotted

Precipitation

Precipitation is monthly surface data in mm from the Climate Research Unit in Norwich (CRU) and available on a 5.0 x 5.0 degree grid from 1900 – 1998. Figure 27 shows the correlation between rainfall and the solar modulated forcing parameters, with only correlations with significance above 90% shown.

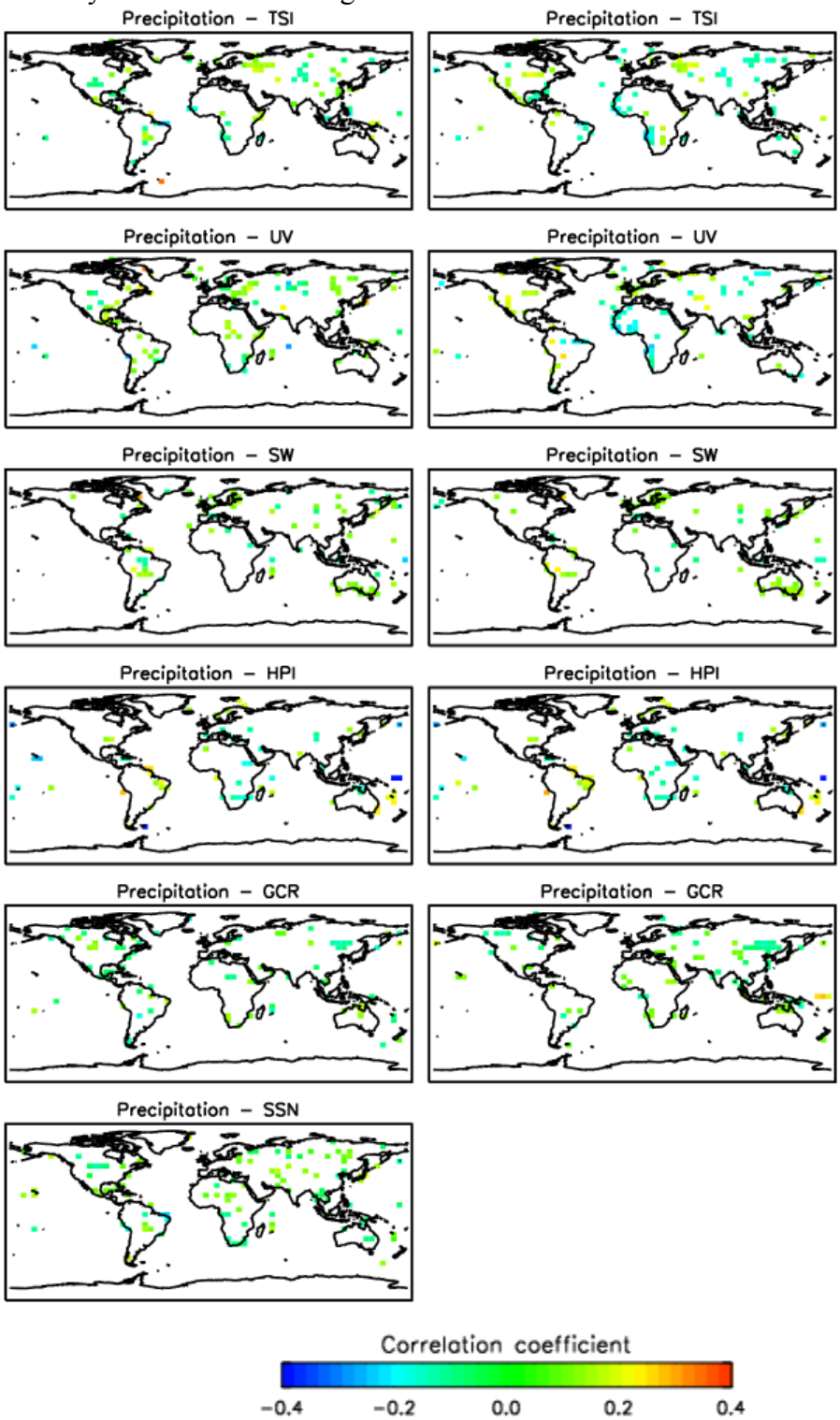

Figure 27: Correlations between the 5 external parameters plus the sunspot number and precipitation. The correlations are given after the removal of the internal parameters and linear trend (left column) and the solar activity (right column). Only the areas with correlation above the 90% significance level have been plotted.

Surface Pressure

The surface pressure is available only for the Northern Hemisphere provided by CRU. This dataset contains monthly mean-sea-level pressure data on a 5° latitude by 10° longitude grid. Figure 30 shows the correlations between surface pressure and the 5 solar modulated forcing parameters. An equivalent pattern is seen in the pictures for TSI, UV, SW, and HPI: a patch of negative correlation in the North Sea/North Atlantic, balanced by positive correlations in the polar regions and further south in the Atlantic. The same pattern is not seen for GCR or SSN. In Figures 28 and 29 we give example of the time series for the surface pressure in selected areas, the North Atlantic and the tropic Pacific where the correlations with TSI and UV differ significantly from 0.

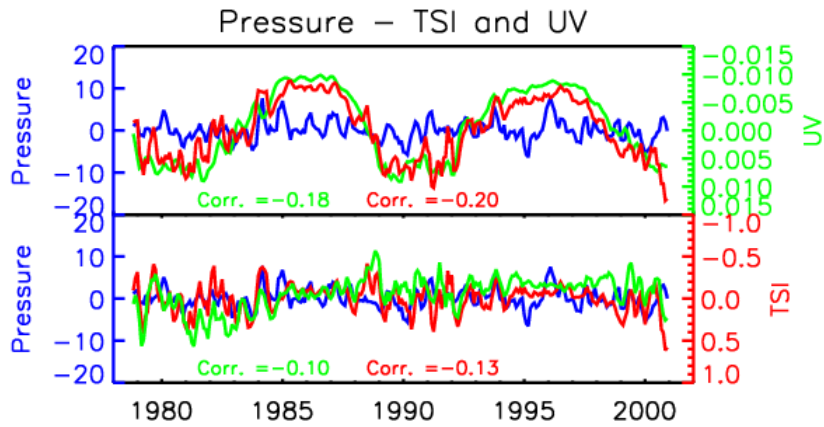

Figure 28: Correlation between surface pressure and TSI and UV in the North Atlantic before removal of the solar cycle (top) and after (bottom).

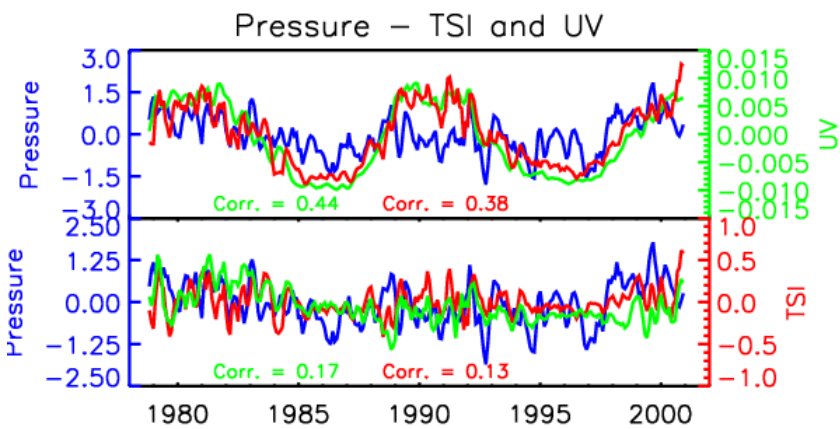

Figure 29: Correlation between surface pressure and TSI and UV in area of the tropic Pacific where the correlation is significantly positive before removal of the solar cycle (top) and after (bottom).

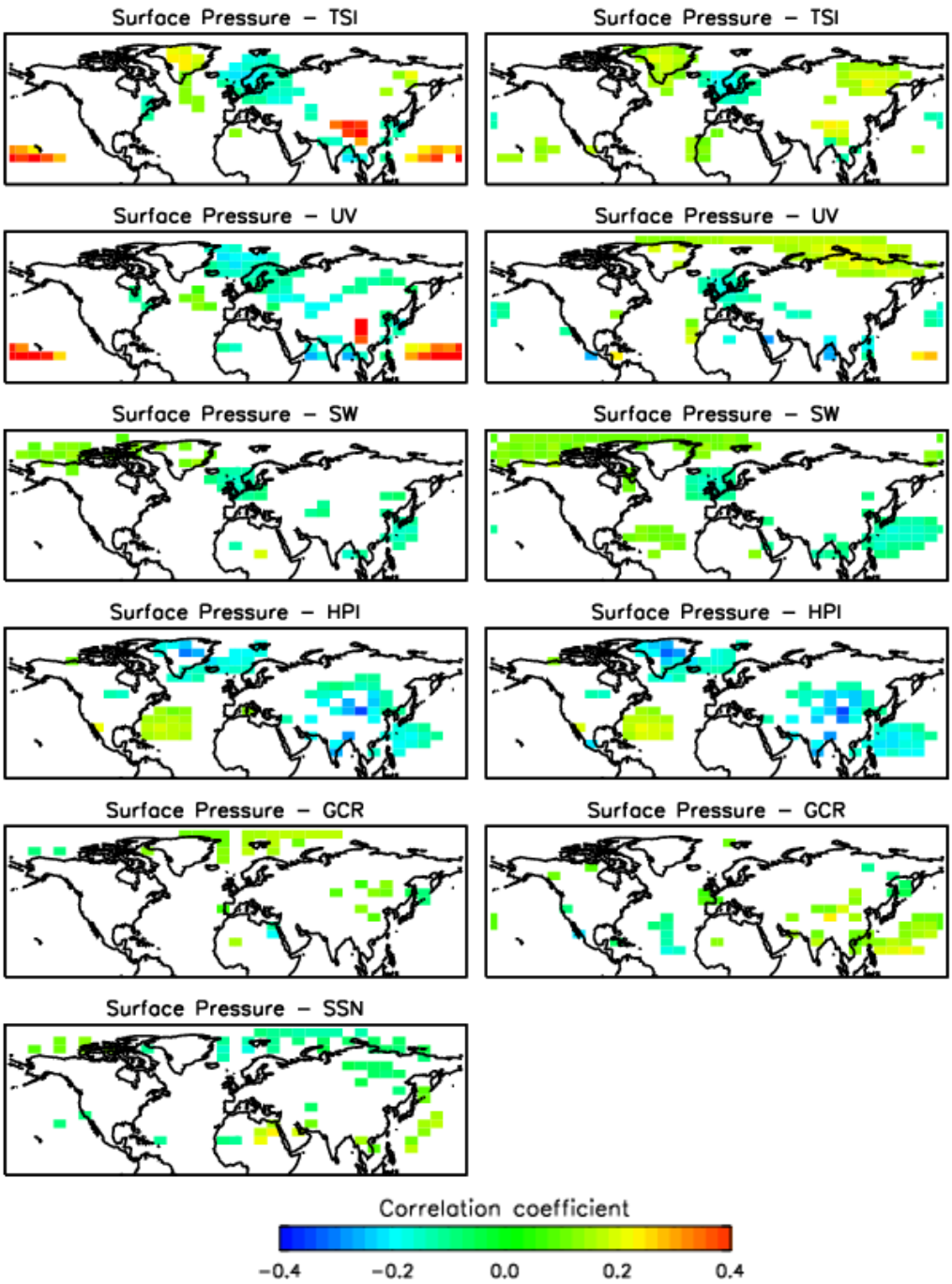

Figure 30 Correlations between the 5 external parameters plus the sunspot number and surface pressure. The correlations are given after the removal of the internal parameters and linear trend (left column) and the solar activity (right column). Only areas with correlations coefficient above the 90% significance level have been plotted.

Surface Temperature

Surface temperature is monthly anomaly data from the Climate Research Unit (air temperature over land) and Hadley Centre (sea surface temperature) and available on a 5.0 x 5.0 degree grid from 1870 – present. Figure 33 shows the correlation between rainfall and the solar modulated forcing parameters, with only correlations with significance above 90% shown. Scattered areas of correlations are observed for all parameters. For GCR these correlations are predominantly negative, whereas there are mixed positive and negative correlations for the other parameters.

In Figures 31 and 32 we present the time series for the global mean surface temperature and global mean sea surface temperature together with the time series for GCR and UV.

In Tables 9 and 10 we give the correlation coefficients for the mean global surface and mean global sea surface temperatures with the 5 external parameters and the sun spot number. EUV and GCR show significant correlations with the surface temperatures, but only for GCR does the correlation survive the removal of the solar cycle.

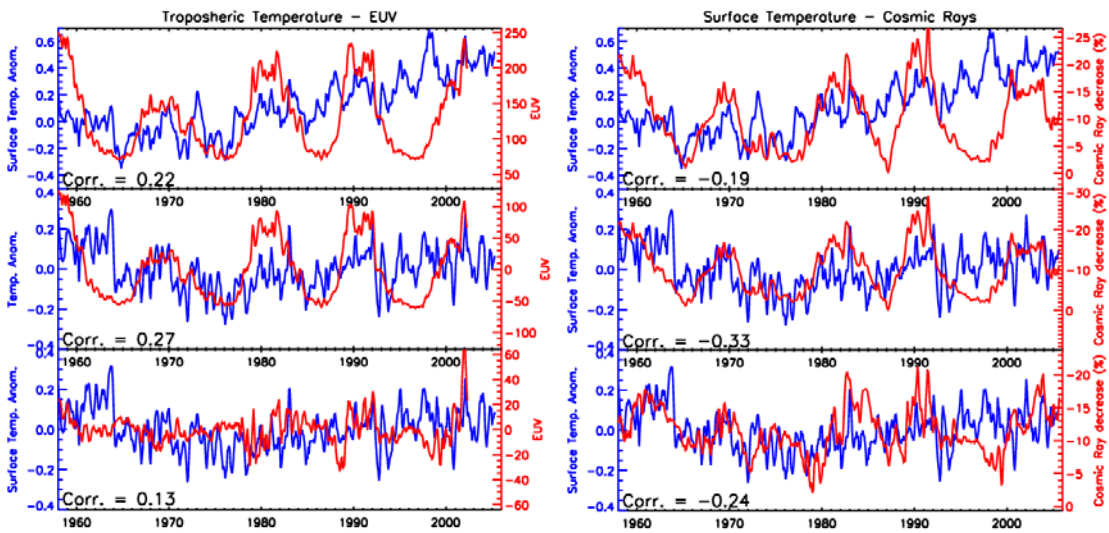

Figure 31: Left) correlation between 10.7 cm EUV proxy and global mean surface temperature anomalies. Top panel: observations. Middle panel: after removal of nino3, NAO, volcanic aerosols, and a linear trend. Bottom: after removal of the solar cycle. Right) the same for galactic cosmic rays.

	TSI	EUV	SW	HPI	GCR	SSN
Observ.	-0.06 (-0.08)	0.22 (0.23)	0.13 (0.19)	-0.11 (-0.12)	-0.19 (-0.20)	0.11 (0.12)
Niño, etc.	**0.21 (0.27)**	***0.27 (0.31)***	0.04 (0.07)	0.00 (0.02)	***-0.33 (-0.38)***	**0.23 (0.27)**
Solar cycle	0.08 (0.07)	0.13 (0.15)	-0.07 (-0.11)	-0.04 (-0.04)	**-0.24 (-0.29)**	

Table 9: The correlations coefficients for the 5 external parameters with surface temperature. Given are the correlations for raw observation, after removal of the internal climate parameters, and after removal of the solar cycle. Numbers in bold face are above the 95% significance level. Numbers in bold italics are above the 99% significance level.

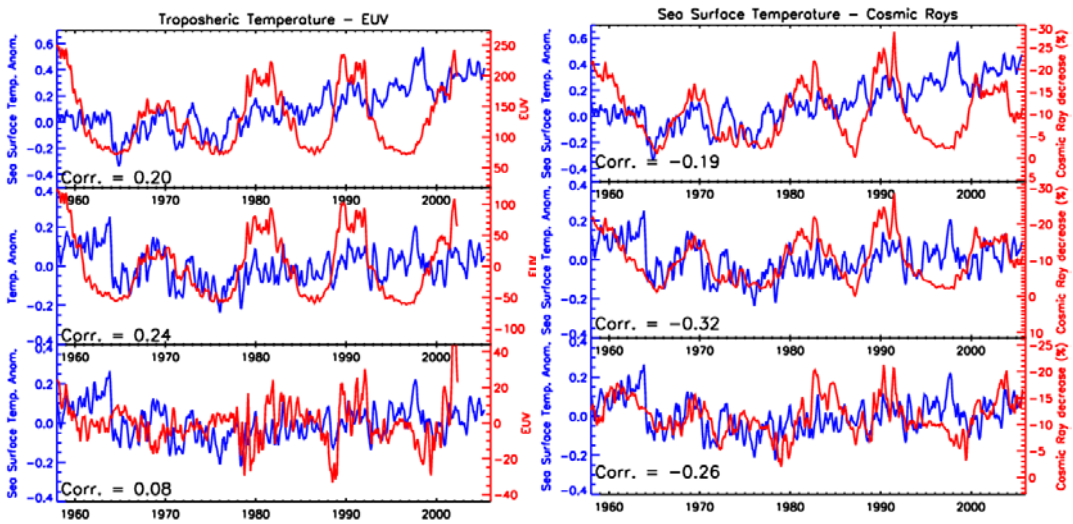

Figure 32: Same as Figure 31, but for sea surface temperatures.

	TSI	EUV	SW	HPI	GCR	SSN
Observ.	-0.17 (-0.20)	0.20 (0.21)	0.12 (0.16)	-0.16 (-0.19)	-0.19 (-0.20)	0.10 (0.12)
Niño, etc.	0.08 (0.09)	0.24 (0.27)	0.04 (0.06)	-0.03 (0.04)	**-0.32 (-0.36)**	0.21 (0.27)
Solar cycle	0.01 (-0.05)	0.08 (0.09)	-0.05 (-0.12)	-0.06 (-0.07)	**-0.26 (-0.30)**	

Table 10: Same as Table 9, but for Sea Surface temperatures.

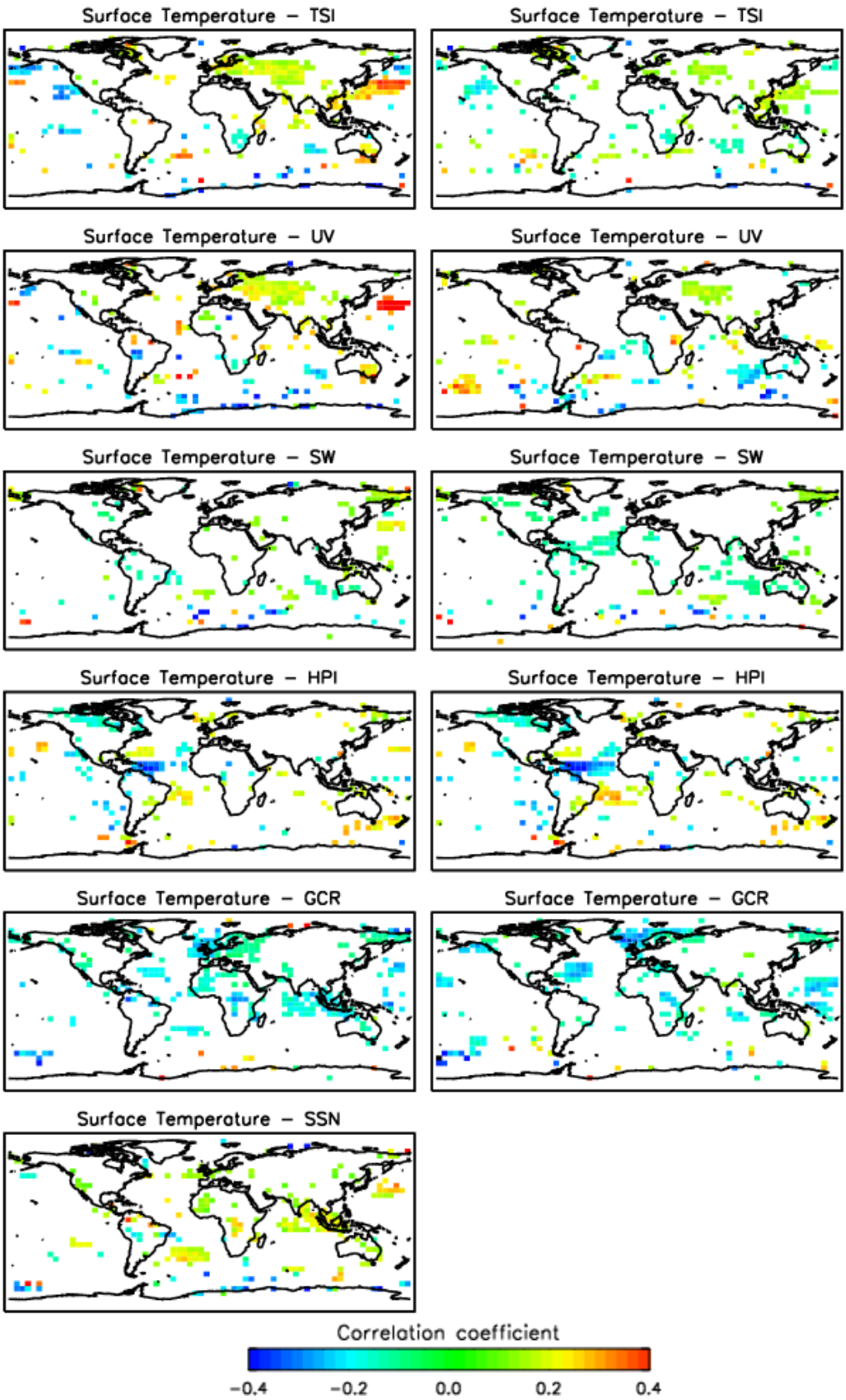

Figure 33: Correlations between the 5 external parameters plus the sunspot number and surface temperature. The correlations are given after the removal of the internal parameters and linear trend (left column) and the solar activity (right column). Only the areas with correlation above the 90% significance level have been plotted

The key results for the surface response for each parameter are:

TSI: very little correlation with the vegetation index, some negative correlation with snow depth, some both positive and negative with precipitation. A pair of negative/positive correlation patches in the North Atlantic/Greenland for surface pressure. Some correlation with surface temperature, that does not, however survive the removal of the solar cycle.
UV: no correlation with vegetation and snow, some with precipitation. A pair of negative/positive correlation patches in the North Atlantic/polar region for surface pressure. Some correlation with surface temperature, that does not, however survive the removal of the solar cycle.
SW: little to no correlation with vegetation, snow or precipitation. A pair of negative/positive correlation patches in the North Atlantic/polar region for surface pressure. Basically no correlation with surface temperature.
HPI: some negative correlation with vegetation. Little to no correlation with snow or precipitation. A pair of negative/positive correlation patches in the North Atlantic/subtropical Atlantic for surface pressure. Basically no correlation with surface temperature.
GCR: negative correlation with vegetation over large parts of the globe. Some correlation with snow, precipitation, and surface pressure. Strongest correlation with surface temperature.
SSN: no correlation with vegetation and snow, some with precipitation, surface pressure and temperature.

The main features are:

- Very little is seen in the correlation between the solar modulated forcing parameters and the various surface parameters, except possibly for surface pressure and for GCR with temperature.
- For TSI, UV, SW, and HPI a patch of negative correlation for surface pressure is observed in the North Atlantic. This is balanced by positive correlation in either the Polar Regions (TSI, UV, and SW) or the subtropical Atlantic (HPI).

Summary

No single solar modulated parameter consistently dominated the response found in each of the climate parameters investigated in this report. The clear majority of solar modulated variability in the various climate parameters could be explained by effects related to the solar cycle. Except for aerosols, all other climate parameters displayed some significant correlation with the solar cycle captured by SSN. However, some significant differences in the strength, sign and spatial distribution of the correlation became apparent once the effects of the solar cycle had been removed. These are potentially the findings that will help give a better constraint on the possible solar modulated mechanisms that are having an impact on tropospheric and surface climate.

The main highlights from the correlation study, once the solar cycle had been accounted for, can be summarised for each of the solar modulated parameters as follows:

TSI

- Zonally averaged temperature under solar min conditions showed some significant positive correlation in the equatorial troposphere.
- No significant correlation was found in any of the other climate parameters.

UV

- Zonally averaged temperatures displayed significant positive correlation coefficients that were comparable to those found with GCR, but then disappeared after removal of the solar cycle.
- Zonally averaged temperatures under solar max/min conditions show a negative/positive correlation in the troposphere, similar, but weaker than, the feature found with GCR.
- Low clouds displayed negative(positive) bands of correlations at mid to high latitudes. These bands were *strengthened* by removal of the solar cycle leading to additional positive(negative) bands of correlation to appear in the tropics.
- Ozone displayed limit areas that were correlated with UV but these were signficantly stronger than with the other solar modulated parameters.
- Aerosols displayed a significant positive correlation in the southern hemisphere.

SW

- Zonally averaged temperature under solar min conditions showed some significant positive correlation in the stratosphere.
- No significant correlation was found in any of the other climate parameters.

HPI

- Zonally averaged temperature under solar min conditions showed some significant negative correlation in the equatorial troposphere.
- Aerosols displayed a significant positive correlation at the equator.
- No significant correlation was found in any of the other climate parameters.

GCR

- Zonally averaged temperatures displayed a significant negative correlation. GCR was the only parameter displaying a significant correlation for global

averages after removal of the solar cycle. However, when limiting the analysis to data after 1978 this correlation disappeared.

- Zonally averaged temperatures under solar max/min conditions show a negative/positive correlation in the troposphere. A similar, but weaker, feature was found with UV, but did not appear with any of the other solar modulated parameters.
- Low clouds displayed negative(positive) bands of correlations at mid to high latitudes similar to UV. The response with UV and GCR was generally very similar and it was difficult to distinguish between these two parameters. However, after removal of the solar cycle the globally averaged correlations were definitely weaker for GCR.
- Aerosols displayed a significant correlation in the southern hemisphere which could not be distinguished from the signal found with UV.

Two final features of note are:

1) That the vertical circulation displayed significant latitudinal bands of positive and negative correlation with all solar modulated forcing parameters after the solar cycle had been removed. However, the latitudinal position of these bands was different for each parameter.
2) Virtually no significant correlation was found in any of the surface climate parameters.

The characteristics outlined in this report now provide a basis for constraining the various solar modulated forcing parameters in the following Tasks.

References

Angell, J. K., Comparison of Variations in Atmospheric Quantities with Sea-Surface Temperature-Variations in the Equatorial Eastern Pacific, *Monthly Weather Review, 109*(2), 230-243, 1981.

Deland, M. T. and R. P. Cebula, Composite Mg-Ii Solar-Activity Index for Solar Cycle-21 and Cycle-22, *Journal of Geophysical Research-Atmospheres, 98*(D7), 12809-12823, 1993.

Ebisuzaki, W., A method to estimate the statistical significance of a correlation when the data are serially correlated, *Journal of Climate, 10*(9), 2147-2153, 1997.

Foster, J. C., J. M. Holt and R. G. Musgrove, Ionospheric Convection Associated with Discrete Levels of Particle-Precipitation, *Geophysical Research Letters, 13*(7), 656-659, 1986.

Frohlich, C. and J. Lean, Solar irradiance variability and climate, *Astronomische Nachrichten, 323*(3-4), 203-212, 2002.

Fullerrowell, T. J. and D. S. Evans, Height-Integrated Pedersen and Hall Conductivity Patterns Inferred from the Tiros-Noaa Satellite Data, *Journal of Geophysical Research-Space Physics, 92*(A7), 7606-7618, 1987.

Hurrell, J. W., Decadal Trends in the North-Atlantic Oscillation - Regional Temperatures and Precipitation, *Science, 269*(5224), 676-679, 1995.

Lockwood, M., An evaluation of the correlation between open solar flux and total solar irradiance, *Astronomy & Astrophysics, 382*(2), 678-687, 2002.

Marsh, N. and H. Svensmark, Galactic cosmic ray and El Nino Southern Oscillation trends in International Satellite Cloud Climatology Project D2 low-cloud properties, *Journal of Geophysical Research-Atmospheres, 108*(D6), 2003.

Peixoto, J. P. and A. H. Oort, Physics of Climate, *Reviews of Modern Physics, 56*(3), 365-429, 1984.

Sato, M., J. E. Hansen, M. P. Mccormick and J. B. Pollack, Stratospheric Aerosol Optical Depths, 1850-1990, *Journal of Geophysical Research-Atmospheres, 98*(D12), 22987-22994, 1993.

Tobiska, W. K., Validating the solar EUV proxy, E-10.7, *Journal of Geophysical Research-Space Physics, 106*(A12), 29969-29978, 2001.

Viereck, R. A. and L. C. Puga, The NOAA Mg II core-to-wing solar index: Construction of a 20-year time series of chromospheric variability from multiple satellites, *Journal of Geophysical Research-Space Physics, 104*(A5), 9995-10005, 1999.

Wallace, J. M., E. M. Rasmusson, T. P. Mitchell, V. E. Kousky, E. S. Sarachik and H. von Storch, The structure and evolution of ENSO-related climate variability in the tropical Pacific: Lessons from TOGA, *Journal of Geophysical Research-Oceans, 103*(C7), 14241-14259, 1998.